J. Fluid Mech. (2003), *vol.* 490, *pp.* 99–127.
DOI: 10.1017/S0022112003005147 Printed in the United Kingdom

Generalized Taylor dispersion in suspensions of gyrotactic swimming micro-organisms

By A. MANELA AND I. FRANKEL

Faculty of Aerospace Engineering, Technion-Israel Institute of Technology, Haifa 32000, Israel

(Received 20 March 2002 and in revised form 2 December 2002)

We calculate the average swimming velocity and dispersion rate characterizing the transport of swimming gyrotactic micro-organisms suspended in homogeneous (simple) shear. These are requisite effective phenomenological coefficients for the macroscale continuum modelling of bioconvection and related collective-dynamics phenomena. The swimming cells are modelled as rigid axisymmetric dipolar particles subject to stochastic Brownian rotations. Calculations are effected via application of the generalized Taylor dispersion scheme. Attention is focused on finite (as opposed to weak) shear. Results indicate that the largest transverse average swimming velocities (essential to gyrotactic focusing) appear shortly after transition from the 'tumbling' mode of motion to cells swimming in the equilibrium direction. At sufficiently large shear rates, dispersivity is not monotonically decreasing with external-field intensity. Exceptional dispersion rates which are unique to non-spherical cells appear in the 'intermediate domain' of external fields. These are rationalized in terms of the corresponding deterministic problem (i.e. in the absence of diffusion) when cell rotary motion is governed by the simultaneous coexistence of multiple stable attractors.

1. Introduction

Gyrotactic focusing (Kessler 1985; Pedley & Kessler 1992) through the balance of gravitational and viscous torques causes bottom-heavy micro-organisms to deviate from the vertical and swim on average towards domains of downwelling. Accumulation of the cells which are denser than the suspending fluid enhances local downward velocity which, in turn, results in further entrainment of cells. Coherent descending plumes of cells are thereby generated and maintained. Thus, unlike the overturning instability in suspensions of purely upswimming micro-organisms and the analogous thermal Rayleigh–Bénard convection, gyrotaxis may lead to spontaneous bioconvection pattern formation even in the absence of a vertical concentration gradient (i.e. in an initially homogeneous suspension). These phenomena may be exploited in a variety of cell-biology-related applications (e.g. rapid concentration of cells, separation of polydisperse populations according to swimming behaviour, etc.). Collective dynamics in suspensions of swimming cells are also significant in ecological and evolutionary issues such as predator–prey balance of species, migration of algal blooms and active transport (e.g. of oxygen) via enhanced mixing (cf. Kessler 1985; Pedley & Kessler 1992).

Continuum macroscale modelling of suspensions of swimming micro-organisms involves (among other things) a conservation equation for $n(\boldsymbol{R}, t)$, the spatial

distribution of cell number density,

$$\frac{\partial n}{\partial t} + \nabla \cdot \bar{\boldsymbol{J}} = 0, \tag{1.1}$$

wherein

$$\bar{\boldsymbol{J}} = [\boldsymbol{V}(\boldsymbol{R}) + \bar{\boldsymbol{U}}]n - \bar{\boldsymbol{D}} \cdot \nabla n. \tag{1.2}$$

In (1.2), $\boldsymbol{V}(\boldsymbol{R})$ is the ambient flow field, $\bar{\boldsymbol{U}}$ denotes the average swimming velocity vector of the micro-organisms and $\bar{\boldsymbol{D}}$ is their effective dispersivity dyadic. The latter coefficient is of prime importance both in linear stability analyses (Bees & Hill 1998; Pedley, Hill & Kessler 1988) as well as in simulations of fully developed bioconvection (Ghorai & Hill 2000).

The first continuum model of suspensions of non-spherical gyrotactic micro-organisms was presented by Pedley *et al.* (1988). They assumed a uniform swimming velocity of the cells in the direction corresponding to the stable equilibrium orientation (existing for a sufficiently weak ambient flow, Pedley & Kessler 1987) and a constant isotropic diffusivity. Pedley & Kessler (1990) pointed out that these assumptions were inconsistent in that the former implied that randomness was weak relative to the orienting gravitational and viscous torques whereas the latter connoted strong randomness. Accordingly, in their later continuum model the effective transport coefficients were obtained via averaging with a probability density function satisfying an appropriate Fokker–Planck equation in orientation space (cf. § 2). Specifically, the present expression of $\bar{\boldsymbol{U}}$, (2.10), is equivalent to their (1.5). The effective cell-diffusivity tensor was defined by a time integral of the covariance of swimming velocity. This definition was subsequently simplified by the postulate of an *ad hoc* (presumed) constant direction-correlation time which apparently allowed for the expression of $\bar{\boldsymbol{D}}$ in terms of the variance of swimming velocity (see (5.1) and (5.2) and the discussion pertaining thereto). Actual calculation of the orientation distribution and the corresponding $\bar{\boldsymbol{U}}$ and $\bar{\boldsymbol{D}}$ was only effected in the limit of (asymptotically) weak ambient shear. While this could be adequate for studying the very onset of instability, the authors indicated that, in order to study fully developed bioconvection and related collective-motion phenomena, it was desirable to calculate the orientation distribution at substantial ambient shear when the hydrodynamic viscous torque was comparable or (asymptotically) large relative to the gravitational torque. (It was further suggested that this would also improve the model of Pedley *et al.* (1988) by relaxing the above-mentioned restriction to deterministic rotary motion dominated by a single stable equilibrium orientation.)

Towards this end Bees, Hill & Pedley (1998) calculated the orientation distribution making use of a Galerkin method (Strand & Kim 1992) truncated at a low order. The distribution thus obtained was then applied to the calculation of $\bar{\boldsymbol{U}}$ and $\bar{\boldsymbol{D}}$ by use of the expressions put forward by Pedley & Kessler (1990). Following Brenner & Weissman (1972), this study was supplemented by an asymptotic calculation for a suspension of spheres at large Péclet numbers under weak gravitational torques. A fairly comprehensive analysis of the orientation distribution of axisymmetric particles was presented by Almog & Frankel (1998) in the context of the rheology of suspensions of dipolar particles. The results in the limit of weak rotary diffusion were rationalized in terms of the corresponding deterministic motion (Almog & Frankel 1995).

Hill & Bees (2002) have recently indicated that a rigorous calculation of $\bar{\boldsymbol{U}}$ and $\bar{\boldsymbol{D}}$ may be accomplished by use of the generalized Taylor dispersion theory (the

expressions employed for $\bar{\boldsymbol{D}}$, their (19) or (32), may, however, not be positive definite at strong shear; see § 5). Towards this end, they have applied the low-order truncated Galerkin scheme of Bees *et al.* (1998) to the calculation of the requisite fields (cf. § 2) for suspensions of spherical cells.

Actual cell-body shapes are often non-spherical (Pedley & Kessler 1992) and the presence of flagella (cf. Jones, LeBaron & Pedley 1994) renders hydrodynamic modelling by spheres still less satisfactory. Moreover, stability analyses (Pedley *et al.* 1988) demonstrate that cell eccentricity significantly affects the resulting dispersion relations. The present contribution is therefore aimed at the calculation of $\bar{\boldsymbol{U}}$ and $\bar{\boldsymbol{D}}$ in sheared suspensions of both spherical and axisymmetric swimming gyrotactic micro-organisms. It is thereby intended to clarify the respective effects on the transport process of such factors as the (finite) shear rate as well as the magnitude and direction of the external field (relative to the ambient shear). Qualitative trends will (as far as possible) be rationalized by reference to the corresponding deterministic rotary motion and orientation distribution previously studied by Almog & Frankel (1995, 1998).

In the next section, the initial- and boundary-value problem governing the motion of a single swimming tracer cell is formulated. Generalized Taylor dispersion theory is then applied to obtain the effective coefficients characterizing the macroscopic transport model problem. Explicit results for the average swimming velocity and dispersion rate are subsequently presented and discussed for spherical and axisymmetric cells (§§ 3 and 4, respectively). Finally, in § 5 we make some comments regarding the applicability and significance of the present results, desirable extensions thereto and the relationship to previous calculations of $\bar{\boldsymbol{D}}$. Asymptotic calculations of the requisite fields are outlined in the Appendix.

2. Formulation of the problem

In a dilute monodisperse suspension, we focus on the motion of a single 'tracer' micro-organism. This, in turn, is modelled as a rigid Brownian axisymmetric-centrosymmetric particle† possessing a permanent embedded dipole (aligned with the axis of symmetry). The instantaneous geometrical configuration of the cell is thus completely specified by $\boldsymbol{R}$, its physical-space position vector and its orientation represented by the unit vector $\boldsymbol{e}$ attached to the dipolar axis (see figure 1). Orientation space may effectively be represented in the present problem by S_2, the unit sphere.

We consider a steady homogeneous shear flow defined by a prescribed constant and uniform ambient velocity gradient dyadic $\boldsymbol{G}$ (see § 5). The present transport problem is thereby decoupled from the dynamic problem. No *a priori* restrictions are imposed on the magnitude of shear rate (represented by G, an appropriate norm of $\boldsymbol{G}$). According to Pedley & Kessler (1990), this is a prerequisite for the discussion of transport phenomena in fully developed bioconvection.

The requisite statistical description of the motion is embodied in $P(\boldsymbol{R}, \boldsymbol{e}, t|\boldsymbol{R}', \boldsymbol{e}')$, the conditional probability density of finding the 'tracer' micro-organism at $(\boldsymbol{R}, \boldsymbol{e})$ at $t > 0$ given that it was introduced at $t = 0$ at the phase-space position $(\boldsymbol{R}', \boldsymbol{e}')$. This density function satisfies the continuity equation

$$\frac{\partial P}{\partial t} + \nabla_{\boldsymbol{R}} \cdot \boldsymbol{J} + \nabla_{\boldsymbol{e}} \cdot \boldsymbol{j} = 0, \tag{2.1}$$

† The results of Jones *et al.* (1994) indicate that this model qualitatively applies to bi-flagellated micro-organisms as well.

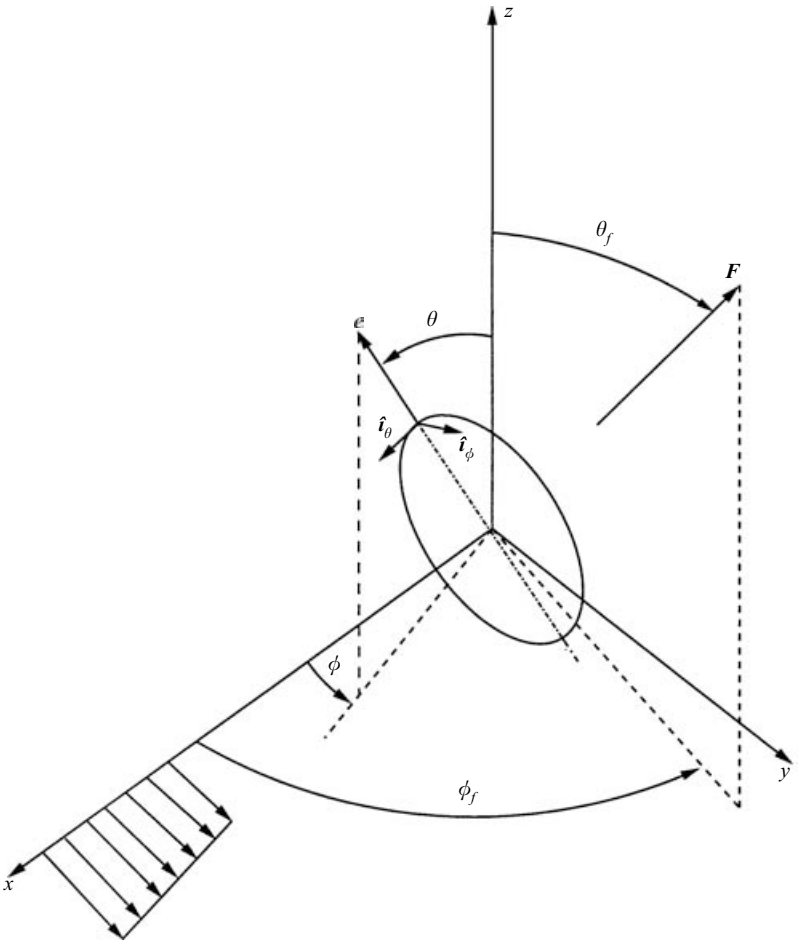

FIGURE 1. Definition of orientation $\boldsymbol{e} \equiv (\theta, \phi)$ of an axisymmetric cell suspended in simple shear flow and subject to an external field acting in the direction $\hat{\boldsymbol{F}} \equiv (\theta_f, \phi_f)$.

to be supplemented by appropriate constitutive equations for the physical- and orientation-space flux-density vectors. The former is

$$\boldsymbol{J} = [\boldsymbol{V}(\boldsymbol{R}') + (\boldsymbol{R} - \boldsymbol{R}') \cdot \mathbf{G} + U\boldsymbol{e}]P, \tag{2.2}$$

wherein $\boldsymbol{V}(\boldsymbol{R}')$ denotes the undisturbed fluid velocity at $\boldsymbol{R}'$. The sum of the first two terms in the square brackets thus represents the contribution of passive convection at the ambient fluid velocity. The last term corresponds to swimming at the instantaneous direction $\boldsymbol{e}$ and presumed uniform speed U. Typically, the settling speed is much smaller than U. The contribution to $\boldsymbol{J}$ of micro-organism sedimentation is therefore neglected relative to that of swimming.

Stochastic changes of swimming direction result from the locomotory motions of the micro-organisms. These changes may either occur as finite discrete velocity jumps or evolve through the accumulation of small gradual rotations which, on the time scale of observation, appear as a continuous change (Othmer, Dunbar & Alt 1988; Dickinson 2000). The former process models the run-and-tumble motion of some chemotactic bacteria. The corresponding stochastic changes of swimming direction

are represented by an integral turning operator, thereby leading to a Boltzmann-like equation for the probability density distribution (Alt 1980; Bearon & Pedley 2000; Hillen & Othmer 2000). In marked contrast to this, the cell-tracking results presented by Hill & Häder (1997) and Vladimirov *et al.* (2000) indicate that gyrotactic cells in a quiescent fluid change their swimming direction in a gradual and continuous manner. This observation, together with the analysis of Hill & Häder (1997), supports the model advanced by Pedley & Kessler (1990). The stochastic elements in the motion of these cells are described as Brownian rotations characterized by a constant effective (transverse) rotary diffusion coefficient d_r (independent of the instantaneous cell orientation). This coefficient is much larger than the corresponding thermal molecular coefficient. (Thus, Pedley & Kessler (1992) mention $d_r \approx 6.7 \times 10^{-2}\,\mathrm{s}^{-1}$ as an effective value for the alga *Chlamydomonas nivalis* whereas application of the Stokes–Einstein relation yields $d_r \approx 1.2 \times 10^{-3}\,\mathrm{s}^{-1}$ for a geometrically similar rigid spheroid.) Following this model, the orientation-space flux density is the sum of convection and diffusion terms

$$\boldsymbol{j} = G\dot{\boldsymbol{e}}P - d_r \nabla_{\boldsymbol{e}} P. \tag{2.3}$$

In (2.3),

$$\dot{\boldsymbol{e}} = \boldsymbol{e}\cdot\hat{\boldsymbol{\Lambda}} + B(\boldsymbol{I} - \boldsymbol{ee})\boldsymbol{e}:\hat{\boldsymbol{S}} + \lambda(\boldsymbol{I} - \boldsymbol{ee})\cdot\hat{\boldsymbol{F}}, \tag{2.4}$$

wherein $\hat{\boldsymbol{S}}$ and $\hat{\boldsymbol{\Lambda}}$, respectively, denote the symmetric and anti-symmetric portions of the dimensionless ambient-velocity gradient $\hat{\boldsymbol{G}} = \boldsymbol{G}/G$ and $\boldsymbol{I}$ is the unit isotropic second-order tensor. The scalar B (α_0 in the notation of Pedley & Kessler 1987) is the intrinsic rotational shear-diffusion coefficient determined by the eccentricity of the axisymmetric particle. Thus, for spheroids, $B = (R^2 - 1)/(R^2 + 1)$ where R is the ratio of polar and equatorial radii (cf. Brenner 1972). The convective portion of orientation space flux thus consists of rotation at the undisturbed fluid angular velocity, the contribution of fluid strain rate to the rotation of the non-spherical cell and the rotary motion resulting from a uniform external field acting in the direction of the unit vector $\hat{F}$. In the latter, appears the parameter

$$\lambda = \frac{m_r F r}{G},$$

in which m_r denotes the hydrodynamic mobility corresponding to particle rotation about a transverse axis; r and F are the respective magnitudes of the dipole moment and external field. As such, λ expresses the relative effects on particle rotation of the external field and fluid shear, respectively. For a spherical cell under gravity, we obtain $\lambda = \rho_c g r/6\,\mu G$ wherein ρ_c denotes the cell density, μ is the carrier-fluid (water) viscosity and g is the acceleration due to gravity. Pedley *et al.* (1988) give $r \approx 10^{-5}$ cm as an approximate value of the centre-of-gravity offset for *C. nivalis*. Typical convection velocities and length scales in steady bioconvection patterns (Bees & Hill 1997; Bees *et al.* 1998; Pedley *et al.* 1988) yield $G \approx 1\,\mathrm{s}^{-1}$ as a representative shear rate in fully developed bioconvection. Combining these data, we estimate $\lambda \gtrsim 0.15$ for *C. nivalis*.

The foregoing continuity and constitutive equations are supplemented by the far-field attenuation condition

$$|\boldsymbol{R} - \boldsymbol{R}'|^m P \to 0 \quad \text{as} \quad |\boldsymbol{R} - \boldsymbol{R}'| \to \infty, \quad m = 0, 1, 2, \ldots, \tag{2.5}$$

the requirements of continuity and single-valuedness in S_2 and the initial condition

$$P = \delta(\boldsymbol{R} - \boldsymbol{R}')\delta(\boldsymbol{e} - \boldsymbol{e}') \quad \text{at} \quad t = 0, \tag{2.6}$$

wherein δ denotes the Dirac distribution. The foregoing problem uniquely determines $P > 0$ (which may serve as the appropriate Green's function for an arbitrary initial distribution replacing the 'instantaneous source' (2.6)).

Actual calculation of P is a formidable task requiring the solution of the above initial- and boundary-value problem formulated within the five-dimensional phase space. However, we are generally not interested in the exhaustively detailed information embodied in the exact solution, but rather only in its orientation average

$$\bar{P}(\boldsymbol{R}, t|\boldsymbol{R}', \boldsymbol{e}') = \int_{S_2} P(\boldsymbol{R}, \boldsymbol{e}, t|\boldsymbol{R}', \boldsymbol{e}')\, \mathrm{d}^2\boldsymbol{e}, \tag{2.7}$$

describing particle transport within physical space irrespective of its instantaneous orientation. Making use of the generalized Taylor dispersion theory (GTDT), a long-time ($t \gg d_r^{-1}$) asymptotic description of $\bar{P}$ may be obtained without the *a priori* calculation of the exact P itself (see Brenner 1980, 1982; Frankel & Brenner 1989, 1991, 1993). Within the framework of this formalism, the requisite $\bar{P}$ is the solution of a physical-space convection–diffusion model problem consisting of the continuity equation

$$\frac{\partial \bar{P}}{\partial t} + \nabla_{\boldsymbol{R}} \cdot \bar{\boldsymbol{J}} = 0, \tag{2.8}$$

and the constitutive equation

$$\bar{\boldsymbol{J}} = [\boldsymbol{V}(\boldsymbol{R}') + (\boldsymbol{R} - \boldsymbol{R}') \cdot \boldsymbol{G} + \bar{\boldsymbol{U}}]\bar{P} - \bar{\boldsymbol{D}} \cdot \nabla_{\boldsymbol{R}} \bar{P}, \tag{2.9}$$

together with the appropriate counterparts of the attenuation (2.5) and initial (2.6) conditions.

Similarly to (1.2), the model constitutive equation (2.9) is characterized by the pair of effective phenomenological coefficients, $\bar{\boldsymbol{U}}$ and $\bar{\boldsymbol{D}}$. According to the GTDT, these coefficients are obtained via the S_2 quadratures

$$\bar{\boldsymbol{U}} = U \int_{S_2} P_0^{\infty}(\boldsymbol{e})\boldsymbol{e}\, \mathrm{d}^2\boldsymbol{e} = U\bar{\boldsymbol{e}} \tag{2.10}$$

(cf. Pedley & Kessler 1990) for the average swimming velocity and

$$\bar{\boldsymbol{D}} = \frac{U^2}{d_r}\left[\int_{S_2} P_0^{\infty}(\boldsymbol{e})[\![B(\boldsymbol{e})\, e]\!]^s\, \mathrm{d}^2\boldsymbol{e} + Pe \int_{S_2} P_0^{\infty}(\boldsymbol{e})[\![B(\boldsymbol{e})\boldsymbol{B}(\boldsymbol{e})\, \mathrm{d}^2\boldsymbol{e} \cdot \hat{\boldsymbol{G}}]\!]^s\right], \tag{2.11}$$

wherein $[\![\cdot]\!]^s$ denotes the symmetric part of the tensor, for the Taylor dispersivity dyadic. The latter coefficient may alternatively be written

$$\bar{\boldsymbol{D}} = \frac{U^2}{d_r} \int_{S_2} P_0^{\infty}(\boldsymbol{e})(\nabla_{\boldsymbol{e}}\boldsymbol{B}(\boldsymbol{e}))^{\dagger} \cdot \nabla_{\boldsymbol{e}}\boldsymbol{B}(\boldsymbol{e})\, \mathrm{d}^2\boldsymbol{e} \tag{2.12}$$

$(\ )^{\dagger}$ denoting the transposed tensor, which (for $P_0^{\infty} > 0$) clearly demonstrates that it is positive-definite. Appearing in (2.11) is the rotary Péclet number

$$Pe = G/d_r$$

expressing the relative effects of shear and rotary diffusion. (From the above-mentioned values of d_r and G, we obtain $Pe \approx 15$ in fully developed bioconvection.)

The scalar $P_0^\infty(\boldsymbol{e})$ and vector $\boldsymbol{B}(\boldsymbol{e})$ orientation-specific fields† appearing in (2.10)–(2.12) satisfy the pair of time-independent orientation-space convection–diffusion problems

$$\nabla_{\boldsymbol{e}} \cdot (Pe\, \dot{\boldsymbol{e}}\, P_0^\infty - \nabla_{\boldsymbol{e}} P_0^\infty) = 0, \tag{2.13}$$

and

$$\int_{S_2} P_0^\infty \, \mathrm{d}^2\boldsymbol{e} = 1; \tag{2.14}$$

$$\nabla_{\boldsymbol{e}} \cdot [Pe\, \dot{\boldsymbol{e}}(P_0^\infty \boldsymbol{B}) - \nabla_{\boldsymbol{e}}(P_0^\infty \boldsymbol{B})] - Pe(P_0^\infty \boldsymbol{B}) \cdot \hat{\mathbf{G}} = P_0^\infty(\boldsymbol{e} - \bar{\boldsymbol{e}}), \tag{2.15}$$

and

$$\int_{S_2} P_0^\infty \boldsymbol{B} \, \mathrm{d}^2\boldsymbol{e} = 0, \tag{2.16}$$

respectively.

In the present problem, Taylor dispersion represents the coupling between the rotary diffusive sampling of orientation-space and orientation dependence of swimming velocity. For typical values of swimming speeds $\approx 10^2$ μm/s^{-1} and cell diameters ≈ 10 μm (Pedley *et al.* 1988), together with the above-mentioned d_r and subsequent results for the eigenvalue of $\bar{\boldsymbol{D}}$ (cf. figures 4 and 7) we estimate $|\bar{\boldsymbol{D}}| \gtrsim 10^{-4}$ cm^2 s^{-1}. This is $\approx 10^6$ times larger than the translational molecular diffusion coefficient obtained from the Stokes–Einstein relation. Translational Brownian diffusion is thus negligible and therefore no counterpart of the effective dispersion term in (2.9) or (1.2) appears in the purely convective physical-space flux (2.2) of the original problem.

We have focused in the following on the simple shear flow

$$\boldsymbol{V} = \hat{\boldsymbol{i}}_2 G x, \tag{2.17}$$

wherein $(\hat{\boldsymbol{i}}_1, \hat{\boldsymbol{i}}_2, \hat{\boldsymbol{i}}_3)$ is a right-handed triad of orthonormal space-fixed unit vectors in the directions of the (x, y, z) axes. Parameterizing $\boldsymbol{e} = (\theta, \phi)$ and $\hat{\boldsymbol{F}} = (\theta_f, \phi_f)$ in terms of the spherical polar and azimuthal angles, the orientation-space gradient operator is

$$\nabla_{\boldsymbol{e}} \equiv \frac{\partial}{\partial \boldsymbol{e}} = \hat{\boldsymbol{i}}_\theta \frac{\partial}{\partial \theta} + \hat{\boldsymbol{i}}_\phi \frac{1}{\sin\theta} \frac{\partial}{\partial \phi}, \tag{2.18}$$

in which $(\boldsymbol{e}, \hat{\boldsymbol{i}}_\theta, \hat{\boldsymbol{i}}_\phi)$ is a right-handed triad of particle-fixed unit vectors (figure 1) and $\dot{\boldsymbol{e}} = \hat{\boldsymbol{i}}_\theta \dot{\theta} + \hat{\boldsymbol{i}}_\phi \dot{\phi} \sin\theta$. Making use of these in (2.4), (2.13) and (2.15) we obtain for P_0^∞ and $b_i (i = 1, 2, 3)$, the scalar components of $P_0^\infty \boldsymbol{B}$,

$$\mathscr{L} P_0^\infty = 0, \quad \int_0^\pi \int_0^{2\pi} P_0^\infty \sin\theta \, \mathrm{d}\phi \, \mathrm{d}\theta = 1, \tag{2.19a, b}$$

$$\mathscr{L} b_i - Pe\, b_1 \delta_{i2} = P_0^\infty (e_i - \bar{e_i}), \quad \int_0^\pi \int_0^{2\pi} b_i \sin\theta \, \mathrm{d}\phi \, \mathrm{d}\theta = 0, \tag{2.20a, b}$$

† From the definitions of P_0^∞ and $\boldsymbol{B}$ in terms of long-time limits of expressions involving the statistical moments of P, we can attribute to these fields the following kinematic significance: P_0^∞ is the steady orientation distribution; $\boldsymbol{B}$ represents the long-time limit of the displacement of the centroid of the sub-population of micro-organisms instantaneously swimming in the direction $\boldsymbol{e}$ relative to the physical-space position of the centroid of the entire population (cf. Frankel & Brenner 1991).

wherein δ_{ij} is the Kronecker delta, $\mathscr{L}$ denotes the differential operator

$$\mathscr{L}f = Pe\left[\frac{1}{\sin\theta}\frac{\partial}{\partial\theta}(\dot{\theta}\sin\theta f) + \frac{\partial}{\partial\phi}(\dot{\phi}f)\right] - \left[\frac{1}{\sin\theta}\frac{\partial}{\partial\theta}\left(\sin\theta\frac{\partial}{\partial\theta}f\right) + \frac{1}{\sin^2\theta}\frac{\partial^2}{\partial\phi^2}f\right], \quad (2.21)$$

$$\dot{\theta} = \tfrac{1}{4}B\sin 2\theta\sin 2\phi + \lambda[\sin\theta_f\cos\theta\cos(\phi-\phi_f) - \cos\theta_f\sin\theta] \quad (2.22a)$$

and

$$\dot{\phi} = \tfrac{1}{2}(1 + B\cos 2\phi) - \lambda\frac{\sin\theta_f}{\sin\theta}\sin(\phi-\phi_f). \quad (2.22b)$$

The symmetry properties of (2.22a,b) allow us to restrict, without loss of generality, the variation of $\hat{\boldsymbol{F}}$ and B to the intervals $0\leqslant\theta_f\leqslant\pi/2$, $0\leqslant\phi_f\leqslant\pi$ and $0\leqslant B\leqslant 1$.

Numerical computation of P_0^∞ and $\boldsymbol{b}$ is effected via application of Galerkin's method similarly to Strand & Kim (1992) (see also Frankel & Brenner 1993; Hill & Bees 2002). Towards this end, the requisite fields are expanded in respective series of surface harmonics

$$f = A_0 + \sum_{n=1}^{\infty}\sum_{m=0}^{n}\left(A_n^m\cos m\phi + B_n^m\sin m\phi\right)P_n^m(\cos\theta).$$

From the normalization conditions (2.19b) and (2.20b), we readily obtain $A_0 = 1/4\pi$ for $f = P_0^\infty$ and $A_0 = 0$ for $f = b_i$ $(i = 1, 2, 3)$. Furthermore, truncation of the series beyond some degree $n = N$, substitution into (2.19a) and use of recurrence relation and orthogonality properties of the associated Legendre functions P_n^m yield a system of $N(N+2)$ linear algebraic equations for the coefficients A_n^m, B_n^m in the expansion of P_0^∞†. Once these are obtained, the forcing terms on the right-hand side of (2.20a) are calculated. The resulting algebraic systems for b_i are then recursively solved (initially for b_1 and b_3 (independently of each other) and subsequently for b_2 (dependent upon b_1)). The average swimming velocity $\bar{\boldsymbol{U}}$ and the first term in the expression (2.11) of $\bar{\boldsymbol{D}}$ only depend upon the first-degree coefficients in the expansions of P_0^∞ and $\boldsymbol{b}$, respectively. Evaluation of the second term on the right-hand side of (2.11) requires a numerical quadrature. The numerical scheme allows for the solution of the problems (2.19)–(2.22) for essentially arbitrary values of λ and Pe. Convergence of the various series becomes slower with increasing λ, B and, to a lesser extent, Pe. (Satisfactory accuracy has been verified for truncation at $N\leqslant 30$ when $\lambda\leqslant 1$, $B\leqslant 0.8$ and $Pe\leqslant 40$.) In view of the above estimate of Pe and the general motivation stated at the conclusion of § 1, emphasis in discussion of subsequent results is placed on cases of strong shear.

Finally, the above problem formulation and numerical scheme are appropriate to the study of arbitrary external field orientations. However, previous studies of the rotary motion of dipolar particles (Hall & Busenberg 1969; Almog & Frankel 1995) and their orientation distribution (Almog & Frankel 1998) indicate that the case of an external field acting in the plane of shear, $\theta_f = \pi/2$, is potentially the most interesting in the present transport problem as well. Subsequent analysis therefore focuses on this case which also accords with the prospective application to bioconvection problems where ambient fluid velocities are essentially vertical.

† Explicit forms of the pertinent equations described as well as other details of the computation are available upon request directly from the authors or the Journal of Fluid Mechanics Editorial office, Cambridge.

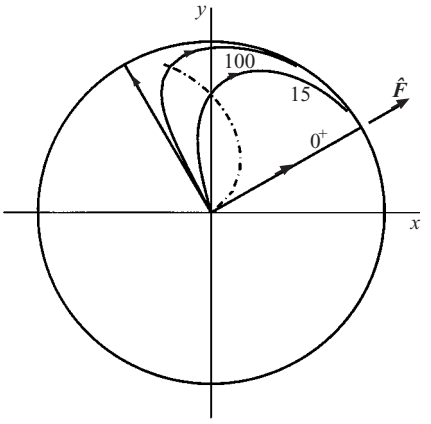

FIGURE 2. Effect of the Péclet number on the variation with λ of the average swimming velocity of spheres. ———, $\bar{U}/U$ at indicated Pe, –·–, locus of $\lambda = 1/2$.

3. Transport of spherical micro-organisms

In the case of spheres $B = 0$ in (2.4) and (2.22*a*, *b*). The ambient strain rate does not affect $\dot{\boldsymbol{e}}$ which is determined by the interplay of undisturbed fluid vorticity and external field. Furthermore, for an external field acting in the plane of shear, $\dot{\boldsymbol{e}}$ depends only upon the relative azimuthal direction $\phi - \phi_f$. (The same is true of P_0^∞ as well, cf. Bees *et al.* 1998.) The deterministic rotary motion $\boldsymbol{e}(t)$ (i.e. in the absence of diffusion) is governed by (2.4) (or, equivalently, (2.22)) viewed as a dynamical system. For future reference, we outline here the modes of the rotary motion (Hall & Busenberg 1969; Brenner 1970). The type, number and location on S_2 of the critical points is exclusively determined by the value of the field parameter λ. Thus, when $\lambda < 1/2$ a pair of centres exist. The resulting rotary motion is accordingly periodic (the so-called 'tumbling', Kessler 1985) during which the vector $\boldsymbol{e}$ traverses on S_2 one of a family of closed orbits encircling either of the centres (Hinch & Leal 1972). For $\lambda \geqslant 1/2$, a single stable node occurs on the 'equator' ($\theta = \pi/2$). In the long-time limit, particles assume the corresponding stable equilibrium orientation.

3.1. $\bar{\boldsymbol{U}}$, *the average swimming velocity*

The steady orientation distribution has been analysed by Brenner & Weissman (1972) and Hinch & Leal (1972) in the context of the rheology of dilute suspensions of dipolar spheres. By symmetry, when $\theta_f = \pi/2$, $\bar{\boldsymbol{e}}$ lies in the plane of shear. Figure 2 presents the effect of the Péclet number on the variation with λ of $\bar{\boldsymbol{U}}/U = \bar{\boldsymbol{e}}$. The variation is explicitly presented by the solid lines for $Pe = 15$ and 100 as well as the respective limits $Pe \to 0$ (with λPe fixed) and $Pe \to \infty$. The arrows indicate the sense of increasing λ along the various lines and the dash-dotted curve marks the locus of $\bar{\boldsymbol{e}}$ at $\lambda = 1/2$. Since, as mentioned above, P_0^∞ depends only upon $\phi - \phi_f$, pictures corresponding to different azimuthal directions of the external field may be obtained through appropriate rigid-body rotations of figure 2. In the absence of an external field, $\lambda = 0$, spherical particle orientations are uniformly distributed. All curves thus originate from $\bar{\boldsymbol{e}} = 0$. All curves likewise converge to $\bar{\boldsymbol{e}} = \hat{\boldsymbol{F}}$ as $\lambda \to \infty$ when all particles align with the external field. (Actual computation for $Pe = 15$ and 100 has been terminated at $\lambda = 1$ and 0.7, respectively.) Between these limits, $|\bar{\boldsymbol{e}}|$ is monotonically

growing with the orientation distribution becoming increasingly concentrated with λ. In the absence of shear, $Pe=0$, orientations are symmetrically distributed about $\hat{\boldsymbol{F}}$, hence $\bar{\boldsymbol{e}}\|\hat{\boldsymbol{F}}$. In the other limit, $Pe\to\infty$, the orientation distribution is closely related to the above-outlined deterministic rotary motion. Thus, when $\lambda<1/2$ the particle orbits on S_2 and the orientation distribution along each of them are both symmetric relative to the meridional plane perpendicular to $\hat{\boldsymbol{F}}$ (Hinch & Leal 1972), hence $\bar{\boldsymbol{e}}\perp\hat{\boldsymbol{F}}$ within the plane of shear. With growing λ, the orientation distribution (A 8) becomes increasingly biased toward $\bar{\boldsymbol{e}}$ and therefore $|\bar{\boldsymbol{e}}|\to 1$ as $\lambda\to 1/2$. With further increase of $\lambda>1/2$, $\bar{\boldsymbol{e}}$ coincides with the direction of the stable node of the deterministic motion. It thus shifts in the clockwise direction along the equator gradually approaching $\hat{\boldsymbol{F}}$ as $\lambda\to\infty$. At all finite Pe, the variation of $\bar{\boldsymbol{e}}$ is intermediate between the above pair of limits.

In view of the mechanism of gyrotactic focusing in vertical shear flows mentioned at the outset, it seems worth noting the variation with λ of the transverse component of $\bar{\boldsymbol{U}}$ perpendicular to $\hat{\boldsymbol{F}}$. In accordance with the foregoing description of the trends of variation of $\bar{\boldsymbol{e}}$, we see that at a given $Pe(\neq 0)$, $|\bar{\boldsymbol{e}}\times\hat{\boldsymbol{F}}|$ is initially increasing and subsequently decreasing with λ. At large Pe, the maximum takes place at $\lambda\gtrsim 1/2$ (marked by the dash-dotted line), i.e. shortly after switching between the above-mentioned modes of deterministic rotary motion.

3.2. $\bar{\boldsymbol{D}}$, *the Taylor dispersivity*

The dispersivity dyadic $\bar{\boldsymbol{D}}$ is represented by its eigenvalues and principal directions. In the absence of both shear and external fields, $\bar{\boldsymbol{D}}$ is isotropic (dispersion only resulting from swimming) and its three eigenvalues are $\nu_i=1/6\,(i=1,2,3)$. By symmetry, when the external field acts in the plane of shear ($\theta_f=\pi/2$) and for arbitrary values of Pe and λ, a pair of mutually perpendicular principal directions lie in this plane (and the third is perpendicular thereto). We here focus on ν, the larger of the pair of corresponding eigenvalues (which is often the largest as well).

The above-mentioned rigid-rotation-type dependence of $\bar{\boldsymbol{e}}$ upon ϕ_f introduces the latter into the respective forcing terms of the b_i equations ($i=1,2$ in (2.20)). It is straightforward to establish that these components of $\boldsymbol{b}$ may be represented by the superposition

$$b_i(\theta,\phi;\phi_f)=\cos\phi_f b_i(\theta,\phi;\phi_f=0)+\sin\phi_f b_i\,(\theta,\phi;\phi_f=\pi/2). \tag{3.1}$$

Consequently, $\bar{\boldsymbol{D}}$ depends upon $\sin\phi_f$, $\cos\phi_f$ and their products. Numerical results indicate, however, no significant qualitative difference in $\bar{\boldsymbol{D}}$ at various values of ϕ_f. We have focused in the following on $\phi_f=\pi/2$ in which case the asymptotic calculations (Appendix) predict the largest dispersion rates for spheres.

The asymptotic calculation in the Appendix yields, in the limit $\lambda\ll 1$ and $Pe\sim O(1)$

$$\nu\sim\frac{8}{3}\frac{5Pe^2+4Pe(Pe^2+4)^{1/2}+16}{(Pe^2+16)^2}+O(\lambda^2), \tag{3.2}$$

together with the corresponding principal direction

$$\hat{\boldsymbol{u}}\sim\left[\frac{Pe+(Pe^2+4)^{1/2}}{2(Pe^2+4)^{1/2}}\right]^{1/2}\left[\frac{2}{Pe+(Pe^2+4)^{1/2}},1,0\right]+O(\lambda^2). \tag{3.3}$$

In the absence of an external field, $\lambda=0$, these results are exact for all Pe. Initially, ν increases with Pe from $\nu=1/6$ at $Pe=0$ to the maximal value $\nu\approx 0.448$ at $Pe\approx 3.31$. With further increasing Pe, ν monotonically attenuates. At $Pe=0^+$, the corresponding eigenvector $\hat{\boldsymbol{u}}$ lies along the principal direction of extension in the

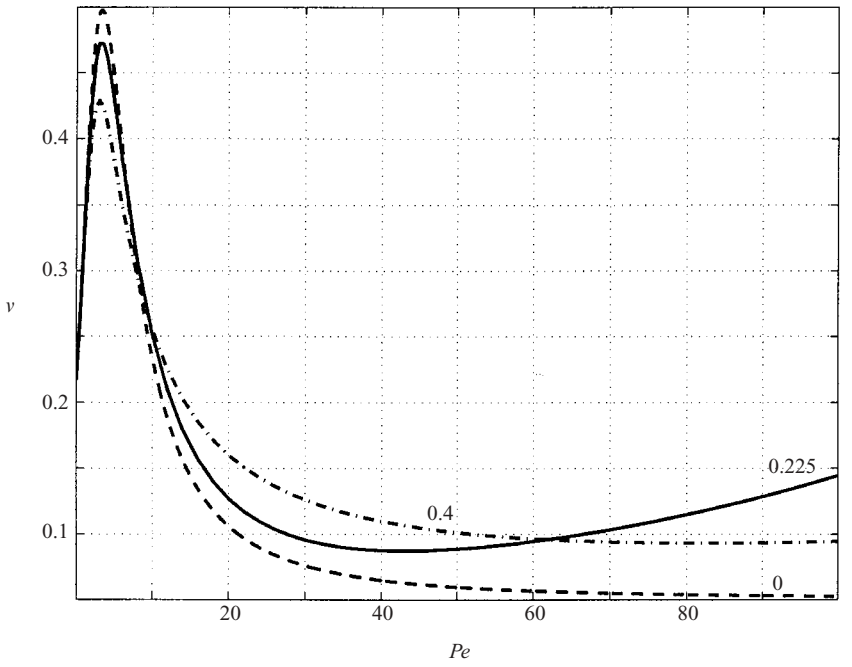

FIGURE 3. Effect of λ on the variation of ν with Pe for spherical cells subject to external field acting in the azimuthal direction $\phi_f = \pi/2$.

ambient flow which suggests that the increased dispersion in the limit of weak shear is generated by the superposition of passive convection on the isotropic swimming (cf. (4.1), (4.2) *et seq.*). Subsequently, with further increasing Pe, $\hat{\boldsymbol{u}}$ gradually approaches the direction of undisturbed fluid velocity indicating that dispersion in the y-direction becomes prominent. This change in $\hat{\boldsymbol{u}}$ essentially results from the growth of the contribution through $\boldsymbol{b}\cdot\hat{\mathbf{G}}$ (in (2.15) or (2.20a)) of b_1, the x-component of $\boldsymbol{b}$, to b_2, the corresponding y-component (see the discussion accompanying (A 5)–(A 7)). Considering the kinematic significance of the vector $\boldsymbol{B}$-field (see the footnote pertaining to (2.15)–(2.16)) we conclude that with increasing shear rate, intense y-dispersion originates from the relative cell displacements in the x-direction coupled with the shear field (2.17).

Figure 3 presents the effects of λ on the variation of ν with Pe, the dashed line corresponding to (3.2) at $\lambda = 0$. Initially, differences are small. All curves start at $\nu = 1/6$ ascending to their respective maxima. These maxima decrease with λ while slightly shifting to smaller Pe. Subsequently, for $Pe \gtrsim 10$ the descent of ν becomes more gradual with increasing λ. At still larger Pe and $\lambda \neq 0$, a minimum appears and ν starts rising again which is most noticeable at $\lambda = 0.225$. The variation of ν with λ thus becomes non-monotonic.

To clarify these trends, figure 4 presents the variation of ν with λ at the indicated values of Pe (thus, along each of these curves, increasing λ corresponds to increasing magnitude of external field). In figure 4(a), we initially recognize trends similar to those mentioned in figure 3. From $Pe = 0$ (the dashed line at $\nu = 1/6$) and up to $Pe \approx 3$, ν is monotonically increasing with Pe and monotonically decreasing with λ. With further increase in Pe, ν starts diminishing and, at $Pe \geqslant 13$, maxima appear at $\lambda \approx 0.4 - 0.5$. From the behaviour observed in figure 3, we anticipate a renewed

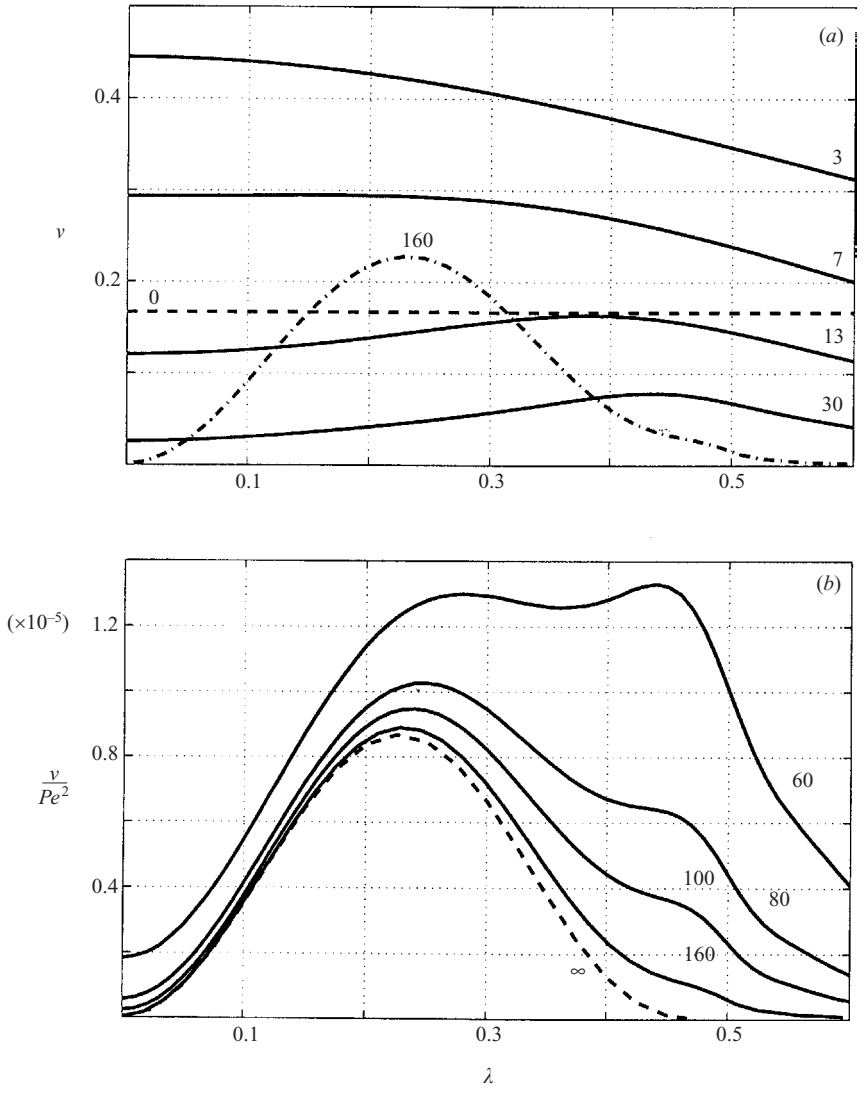

FIGURE 4. Effect of Pe on the variation of ν with λ for spheres subject to external field acting in the direction $\phi_f = \pi/2$. (a) Moderate, (b) large values of Pe.

growth of ν at still larger values of Pe. Indeed, as depicted by the dash-dotted curve, ν is eventually growing and a maximum is apparent at $\lambda \approx 0.225$. An asymptotic calculation in the limit $Pe \gg 1$ and $\lambda \leqslant 1/2$ (see Appendix) yields

$$\nu/Pe^2 \sim \nu_\infty(\lambda) \sin^2 \phi_f + O(Pe^{-1}), \quad \hat{\boldsymbol{u}} \sim (0, 1, 0). \tag{3.4a,b}$$

Figure 4(b) accordingly presents the variation of ν/Pe^2 with λ at $Pe \gg 1$. The solid lines are obtained by numerical computation at the indicated values of Pe. The dashed curve is the asymptote $\nu_\infty(\lambda)$ (3.4a). At $Pe = 60$, a secondary maximum becomes visible at $\lambda \approx 0.28$. With increasing Pe, the original maxima gradually disappear and the solid curves approach the asymptote. We further elaborate on the non-monotonic variation of ν with λ in the context of the dispersion of non-spherical cells.

4. Transport of axisymmetric cells

We here consider the effects of departures from the spherical shape on the average swimming velocity and dispersion rate of swimming micro-organisms. The deterministic rotary motion of axisymmetric dipolar particles may be both qualitatively and quantitatively different from the corresponding motion of dipolar spheres briefly described at the beginning of the preceding section. Thus (cf. Almog & Frankel 1995), for relatively weak external fields (i.e. small λ) acting in the plane of shear, particles either approach a stable limit cycle or stable focal points according to whether ϕ_f is smaller or larger than $\pi/2$. Under the action of sufficiently strong external fields, particles converge to a single stable equilibrium orientation on the equator of S_2 (i.e. on the unit circle $\theta = \pi/2$). Between these 'small' and 'large' values of λ, there may exist an intermediate domain whose extent depends on both ϕ_f and the intrinsic shape parameter B. In this domain, multiple stable attractors may simultaneously coexist or else orientation space may be divided into separate domains wherein different modes of rotary motion occur. These differences in the deterministic rotary motion show up in the following description of the effective phenomenological transport coefficients.

4.1. $\bar{\boldsymbol{U}}$, *the average swimming velocity*

Figure 5 presents the effect of ϕ_f, the azimuthal direction of external field on the variation of $\bar{\boldsymbol{U}}/U = \bar{\boldsymbol{e}}$ with λ. The solid curves describe the variation of $\bar{\boldsymbol{e}}$ in the plane of shear at $Pe = 0^+$, 15 and 100 and the arrows indicate the sense of increasing λ. The open circles denote the projections on the plane of shear of the stable nodes of the corresponding deterministic rotary motion together with the relevant values of λ. The corresponding locations of $\bar{\boldsymbol{e}}$ are marked by asterisks on the respective curves pertaining to $Pe = 100$. In general, with the exception of $\phi_f = 95^\circ$ (which occurs within the above-mentioned intermediate domain, cf. the discussion of figure 10), two nodes are presented for each ϕ_f, respectively corresponding to the smallest value of λ when a stable node initially appears and the (largest) value of λ where the curve pertaining to $Pe = 100$ terminates (all the curves of $Pe = 15$ terminate at $\lambda = 1$).

Similarly to the case of spheres (cf. figure 2), all curves start at $\lambda = 0$ from the origin (while here the orientation distribution is non-uniform even in the absence of an external field, it still possesses three mutually perpendicular planes of symmetry which ensures the vanishing of $\bar{\boldsymbol{e}}$). All curves likewise converge at large λ to $\bar{\boldsymbol{e}} = \hat{\boldsymbol{F}}$. In the absence of shear, $Pe = 0$, $\bar{\boldsymbol{e}} \| \hat{\boldsymbol{F}}$. The figures corresponding to the various values of ϕ_f exhibit both qualitative and quantitative differences and unlike the case of spheres cannot be obtained from each other via appropriate 'rigid-body' rotations.

Focusing on the curves pertaining to $Pe = 100$, we initially observe only relatively minor changes of the azimuthal direction of $\bar{\boldsymbol{e}}$ with λ increasing from $\lambda = 0$ at the origin nearly up to the points marked by the asterisks. Subsequently, following the first appearance of a stable node, $\bar{\boldsymbol{e}}$ veers off rapidly approaching the direction of $\hat{\boldsymbol{F}}$. Similarly to spheres, the largest values of the component of $\bar{\boldsymbol{U}}$ perpendicular to $\hat{\boldsymbol{F}}$ (which is essential in gyrotactic focusing) occur at λ slightly larger than those corresponding to the first appearance of stable equilibrium orientations. With the exception of $\phi_f = 95^\circ$ these, however, take place at λ considerably smaller than 1/2.

Figure 6 presents the variation of $|\boldsymbol{U}|/U$, the (dimensionless) average swimming speed, with λ at $Pe = 15$ (figure 6*a*) and 100 (figure 6*b*). At both values of Pe, the average swimming speed at $\phi_f = 95^\circ$ is significally smaller than at all other values

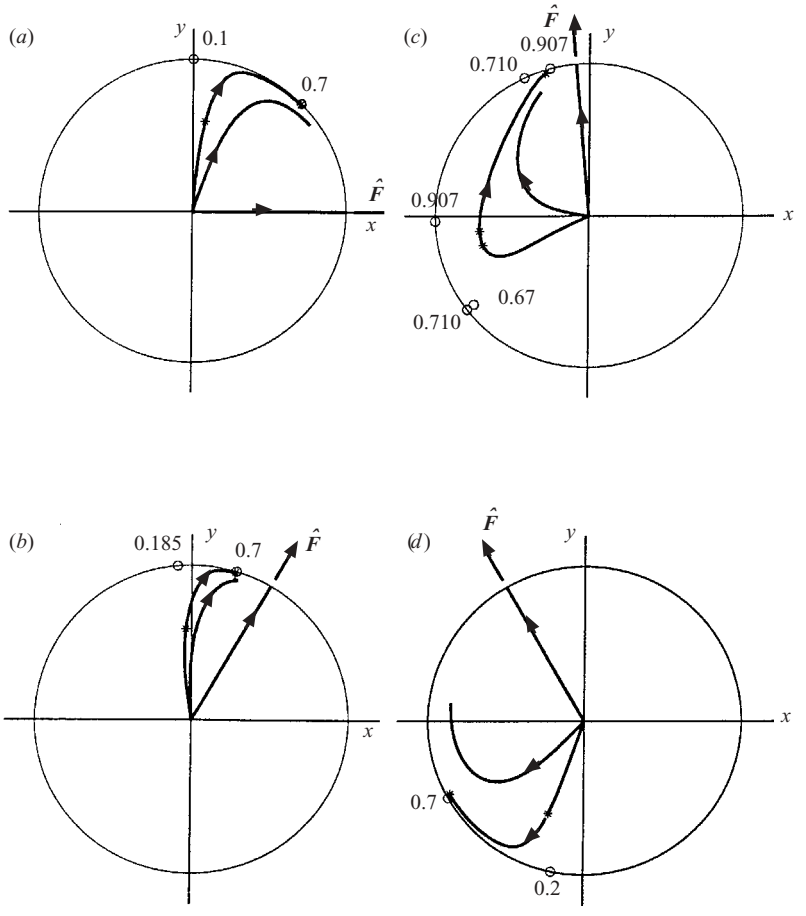

FIGURE 5. Variation with λ of dimensionless average swimming velocity of axisymmetric cells ($B = 0.8$) at $Pe = 0, 15$ and 100 and (*a*) $\phi_f = 0°$, (*b*) 60°, (*c*) 95° and (*d*) 120°. ○, locations of stable nodes of the deterministic problem at indicated values of λ; *, corresponding $\bar{\boldsymbol{e}}$ for $Pe = 100$.

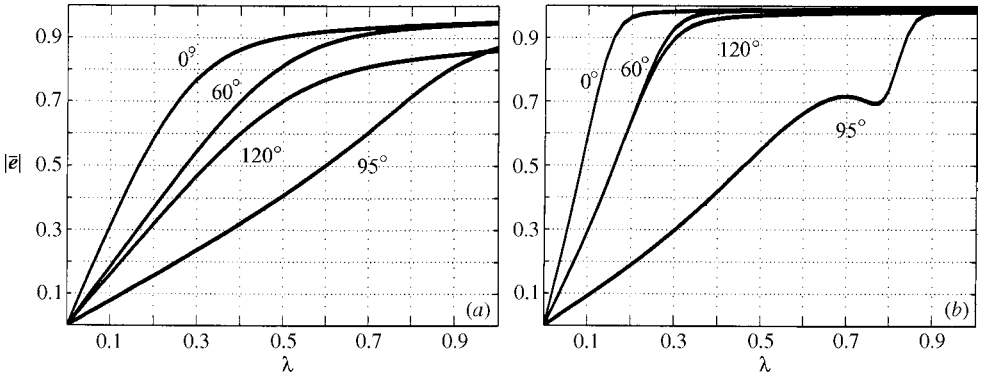

FIGURE 6. Variation of $|\bar{\boldsymbol{e}}|$ with λ for axisymmetric cells ($B = 0.8$) at indicated values of ϕ_f and (*a*) $Pe = 15$ and (*b*) 100.

of ϕ_f presented. Furthermore, at $Pe = 100$ the ascent of $|\boldsymbol{U}|/U$ is non-monotonic for $\lambda \gtrsim 0.7$. Referring back to figure 5(*c*), we note that for $0.71 \leqslant \lambda \leqslant 0.9$, a pair of stable nodes simultaneously coexist. This has a profound effect on the resulting orientation distribution and hence on the average swimming speed (as well as the effective rate of dispersion, see figure 9 and the discussion pertaining thereto.) (Also in this context, Pedley & Kessler (1987, 1992) speculate on potential implications of the existence of a pair of stable equilibria in pure straining flows.)

4.2. $\bar{\boldsymbol{D}}$, *the Taylor dispersivity*

Similarly to the dispersion of spheres, we here focus also on the eigenvalue ν and the corresponding eigenvector $\hat{\boldsymbol{u}}$ characterizing $\bar{\boldsymbol{D}}$. Brenner & Condiff (1972, 1974) studied the orientation distribution of dipolar axisymmetric particles suspended in a general weak homogeneous shear flow and subject to a weak external field. Making use of $\boldsymbol{P_n}(\boldsymbol{e})$, the polyadic surface harmonics (Brenner 1964), they obtained $P_0^{\infty}(\boldsymbol{e})$ in invariant form. Following their scheme, $\boldsymbol{b}(\boldsymbol{e})$ is expanded in powers of Pe and λPe. For the simple homogeneous shear (2.17), we obtain, in the limit $Pe \sim o(1)$ and a fixed $\lambda \sim O(1)$,

$$\nu \sim \tfrac{1}{6} + \tfrac{1}{24}(2+B)Pe + \tfrac{1}{6}\left\{\tfrac{3}{16} + \tfrac{1}{5}B - \tfrac{59}{1680}B^2 - \tfrac{1}{180}\left[83 + \tfrac{29}{12}(2+B)\sin 2\phi_f\right]\lambda^2\right\} Pe^2 \quad (4.1)$$

together with the eigenvector

$$\hat{\boldsymbol{u}} \sim \left[1, 1 + \frac{1}{15(2+B)}\left(\frac{30+29B}{2} + \frac{29\lambda^2}{6}\left(-\cos 2\phi_f + \tfrac{1}{12}(10-B)\sin 2\phi_f\right)\right)Pe + \frac{29\lambda^2(30+29B)}{2700(2+B)^2}\sin 2\phi_f Pe^2, 0\right]. \quad (4.2)$$

The leading-order effect is a (linear) increase of ν with Pe. Within the same order, the corresponding eigenvector lies along the principal direction of extension in the ambient simple shear. The corresponding invariant expression for an arbitrary (weak) homogeneous shear is

$$\bar{\boldsymbol{D}} \sim \tfrac{1}{6}\left[\boldsymbol{I} + Pe\left(1 + \tfrac{1}{2}B\right)\hat{\boldsymbol{S}} + O(Pe^2)\right]. \quad (4.3)$$

This expression indicates (cf. (3.3) *et seq.*) that increased dispersion in the present limit originates from the superposition of the passive distortion of the suspension by the ambient strain and the essentially isotropic swimming of the cells. At a given Pe, ν is decreasing with λ.

The variation of ν with λ at finite values of Pe is depicted by the solid lines in figure 7 for $B = 0.8$ and $\phi_f = 60^\circ$. The dashed line at $\nu = 1/6$ corresponds to the isotropic case at $Pe = 0$. We first observe that the above-mentioned trends (namely the growth of ν with Pe at a given value of λ and its diminution with increasing λ at a constant Pe) persist nearly up to $Pe \approx 7$. At the same time, with increasing Pe, the corresponding eigenvector $\hat{\boldsymbol{u}}$ (which is not presented here) moves counterclockwise, gradually approaching the direction of fluid velocity. This suggests a change in the kinematics of dispersion, similar to that discussed in § 3 (cf. (3.3) *et seq.*).

At still larger values of $Pe \gtrsim 7$, qualitatively different modes of variation of ν appear. To begin with we observe that ν is now decreasing with Pe. Occurrence of a maximum at intermediate values of Pe and subsequent descent of ν has been observed for spheres (cf. figure 4). Unlike spheres, however, no comparable renewed growth of ν takes place at large Pe numbers and λ sufficiently small ($< 1/2$). This difference originates from the orientation distribution of axisymmetric particles at large Pe and

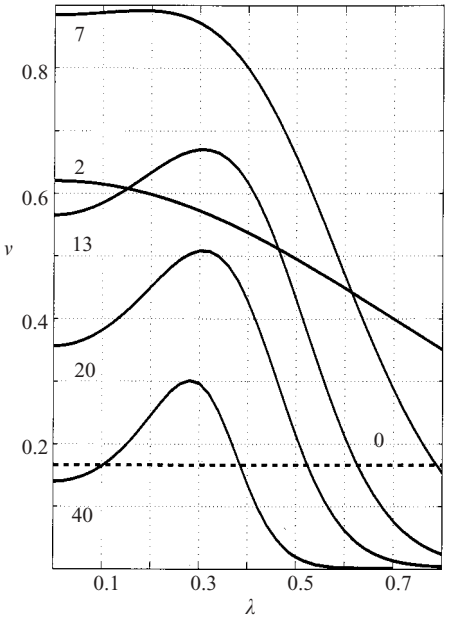

FIGURE 7. Variation of ν with λ for axisymmetric cells ($B = 0.8$) subject to an external field acting in the azimuthal direction $\phi_f = \pi/3$ at the indicated values of Pe.

arbitrarily small λ becoming increasingly concentrated in a boundary layer about the stable attractor (e.g. a limit cycle) of the corresponding deterministic problem (Almog & Frankel 1998).

Less intuitive is the appearance of respective maxima in the variation with λ. Apparently we anticipate that, with growing intensity of external field, P_0^∞ becomes increasingly concentrated about the average orientation (which, in turn, approaches $\hat{\boldsymbol{F}}$, see figure 5). This is expected to result in the diminishing of the forcing term of the $\boldsymbol{B}$-field equation (2.15) and consequently of $\boldsymbol{B}$ and $\bar{\boldsymbol{D}}$ as well. While for very large values of λ, ν indeed eventually vanishes (approximately as $(\lambda Pe)^{-2}$, Manela 2002), for Pe sufficiently large this process is non-monotonic.

Some insight into this behaviour is gained by considering the fields P_0^∞, B_2 (the component of $\boldsymbol{B}$ in the direction of ambient fluid velocity) and the product $P_0^\infty(\nabla_{\boldsymbol{e}} B_2)^2$. Numerical evidence indicates that this product forms the main contribution to ν within the present range of parameter values. To simplify the description, figure 8 presents only the variation of these fields with the azimuthal direction ϕ for particle orientations within the plane of shear ($\theta = \pi/2$), i.e. along the equator of the unit sphere.

Figure 8(a) presents the corresponding sections of P_0^∞. At $\lambda = 0$, this distribution consists of two identical peaks π apart from each other (the entire distribution being invariant under π-translation in ϕ, cf. Almog & Frankel 1998). With increasing intensity of external field, it, on the average, transfers particles from the vicinity of the right-hand peak to that of the left-hand one (being closer to ϕ_f, cf. the discussion of figure 5). This enhancement of the left-hand peak is accompanied by only a slight shift towards ϕ_f.

Figure 8(b) depicts the effect of λ on B_2. Two maxima of $\partial B_2/\partial\phi$ are discernible. With increasing λ, the relatively milder slope on the right-hand side changes only

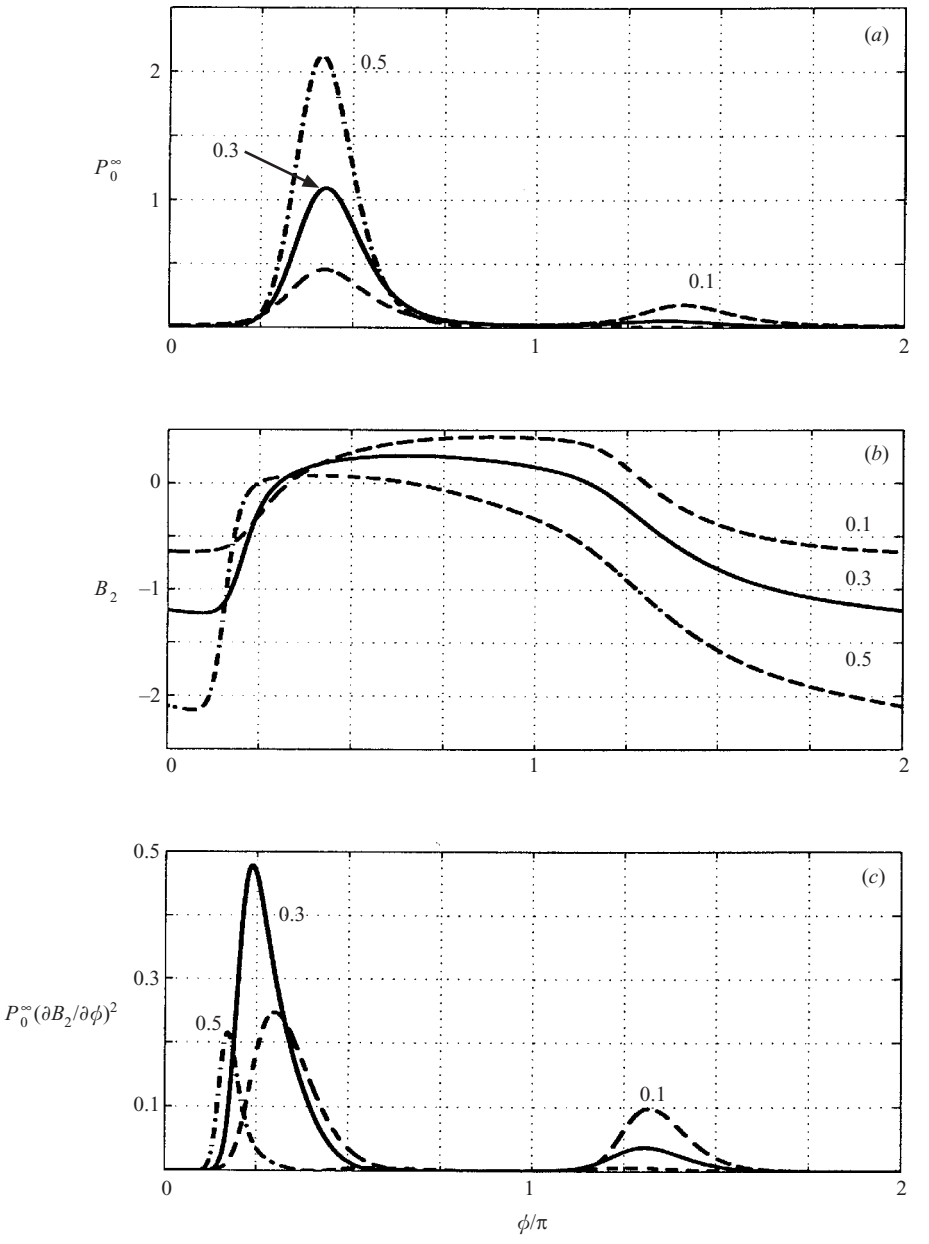

FIGURE 8. Equatorial sections (at $\theta = \pi/2$) of (*a*) P_0^∞, (*b*) B_2 and (*c*) $P_0^\infty(\partial B_2/\partial\phi)^2$ at the indicated values of λ for axisymmetric cells ($B = 0.8$); $Pe = 20$, $\phi_f = \pi/3$.

slightly in magnitude and remains nearly in phase with the right-hand peak of P_0^∞. The sharper left-hand slope is ever steepening with increasing λ. At the same time, this peak is shifting to smaller ϕ, thus becoming out of phase with the corresponding peak of P_0^∞.

These trends are compounded in figure 8(*c*). The smaller contribution of the right-hand peak is monotonically decreasing with λ as a result of P_0^∞ diminishing in this

ϕ interval. The main contribution to the dispersivity comes from the left-hand peak. Here, the steepening of the B_2-gradients and their continual shifting to the left give rise to opposing effects. Initially, when λ grows from 0.1 to 0.3, the former effect prevails, leading to a substantial increase in dispersion. Subsequently, with further increase of λ from 0.3 to 0.5, the gradients of B_2 become even steeper. However, very few particles are present in the relevant domain of orientation space. Dispersion is therefore rapidly diminishing, despite continued intensification of the B_2-gradients. It is only at still larger values of λ that these very gradients start to diminish and eventually vanish. Thus, contrary to earlier presumption, it is the lack of coherence between $\nabla_e \boldsymbol{B}$ and the orientation distribution (rather than decreasing $\nabla_e \boldsymbol{B}$) which brings about the diminution of dispersion.

We now turn to consider the effect on dispersion of ϕ_f, the azimuthal direction of the external field in the plane of shear. Towards this end, figure 9 presents the variation of ν with λ for $B = 0.8$ at the three indicated values of Pe and six values of ϕ_f. Figures 9(a) and 9(f) are qualitatively similar to the previously presented figure 9(b) ($\phi_f = 60^\circ$, cf. figure 7). In fact, quantitative differences are, too, relatively minor. A number of qualitative and quantitative differences are conspicuous at $\phi_f = 95^\circ$, particularly at the larger Péclet numbers presented (figures 9(c) and 9(e) qualitatively depict the transitions between figure 9(d) and the former group).

At $\phi_f = 95^\circ$, we observe the sharp maxima whose values increase with Pe. These values are an order of magnitude larger than the corresponding maxima appearing at $\phi_f = 0^\circ, 60^\circ$ and 135°. Furthermore, the present maxima at $\phi_f = 95^\circ$ occur at $\lambda \approx 0.8$, at which value the corresponding values of ν have already become negligible in figures 9(a), 9(b) and 9(f). No counterpart of this unique behaviour exists in the dispersion of spheres discussed in the preceding section. This behaviour is enhanced with increasing eccentricity of cell shape. For the present $B = 0.8$, it is observed for external field directions ranging from ϕ_f nearly 90° through about 120°.

To clarify the foregoing observations, we present in figure 10 'equatorial sections' of P_0^∞, B_2 and the product of P_0^∞ by $(\partial B_2/\partial\phi)^2$ at the indicated Péclet numbers and $\phi_f = 95^\circ$, $\lambda = 0.8$ (which is in the vicinity of the maxima in figure 9d). Also presented for comparison are the corresponding sections at $\phi_f = 60^\circ$ and $\lambda = 0.3$.

We first note the orientation distribution which for $\phi_f = 95^\circ$ is remarkably different from that of figure 8(a). Even at the relatively large Péclet numbers presented, P_0^∞ is not a narrow boundary-layer type distribution. Rather, significant densities occur over a wide interval of azimuthal angles. Furthermore, with increasing Pe, a secondary peak is emerging. These unique features are related to the occurrence of the above-mentioned 'intermediate domain' of external field directions and magnitudes in which domain of ϕ_f and λ the deterministic rotary motion of spheroids is affected by the simultaneous coexistence of multiple stable equilibrium orientations. Thus, at $\phi_f = 95^\circ$ a pair of stable nodes exist for λ between 0.710 and 0.907 (cf. figure 5 and the discussion pertaining thereto).

Figure 10(c) for $\phi_f = 95^\circ$ shows in the same interval of ϕ, large gradients of B_2 which are still intensifying with Pe. Owing to the peculiar nature of the corresponding P_0^∞, these gradients appear where significant densities exist (unlike all other cases, when the B_2 gradients only appear at the outer margins of P_0^∞). As shown in figure 10(f), the combination of these P_0^∞ and B_2 results in large values of the product $P_0^\infty(\partial B_2/\partial\phi)^2$ throughout a considerable portion of orientation space. Furthermore, these are significantly growing with Pe, leading to substantially enhanced dispersion.

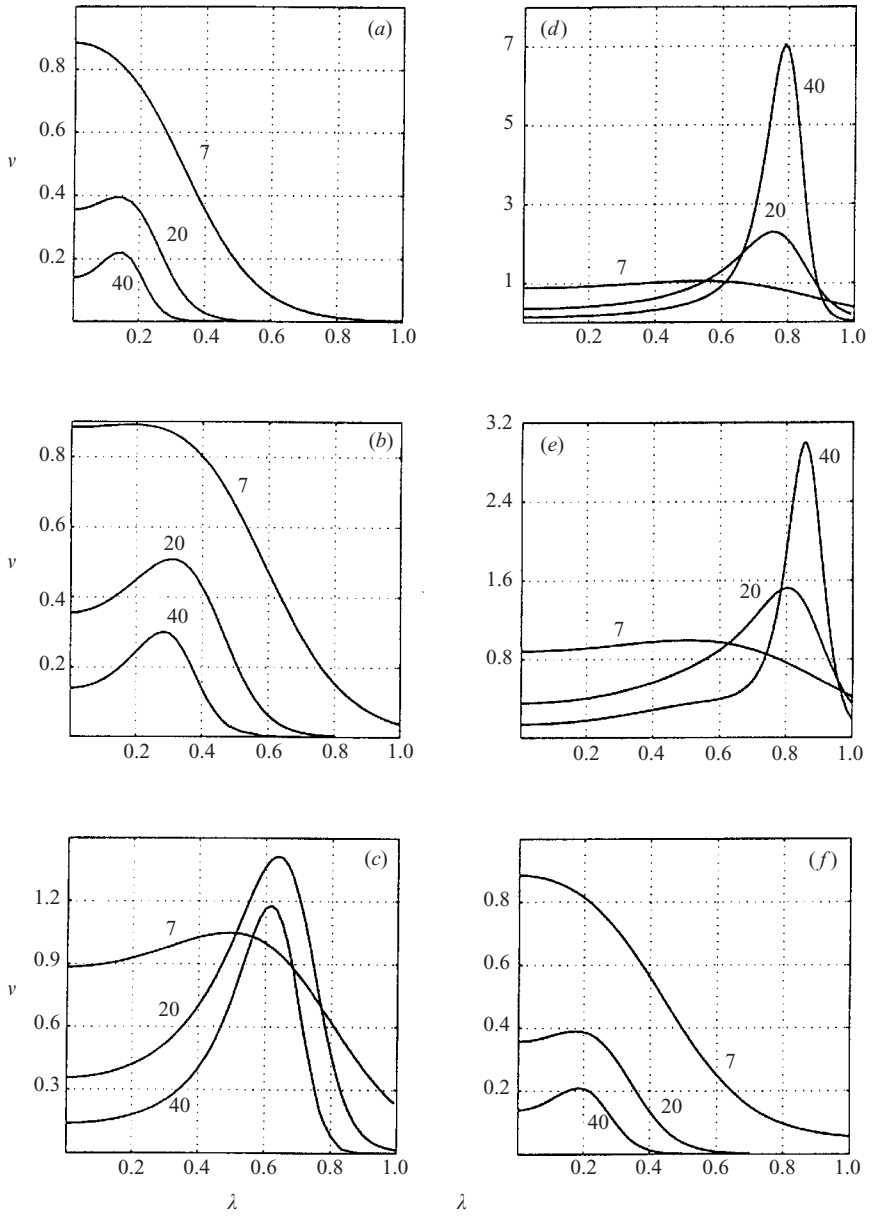

FIGURE 9. Variation of v with λ at the indicated values of Pe and (*a*) $\phi_f = 0°$, (*b*) 60°, (*c*) 84°, (*d*) 95°, (*e*) 100°, (*f*) 135° for axisymmetric cells ($B = 0.8$).

5. Concluding remarks

To begin with, we consider the soundness of the assumed steadiness and homogeneity of the ambient flow. The latter assumption is necessary for the application of the generalized Taylor dispersion theory. (This scheme is based on the recursive calculation of statistical moments which is not possible in the present transport problem unless the carrier-fluid velocity $\boldsymbol{V}$ depends linearly upon $\boldsymbol{R}$.) Furthermore, existence of the macroscopic purely physical space description (2.8) and (2.9) is only guaranteed provided that the eigenvalues of $\mathbf{G}$, the velocity gradient,

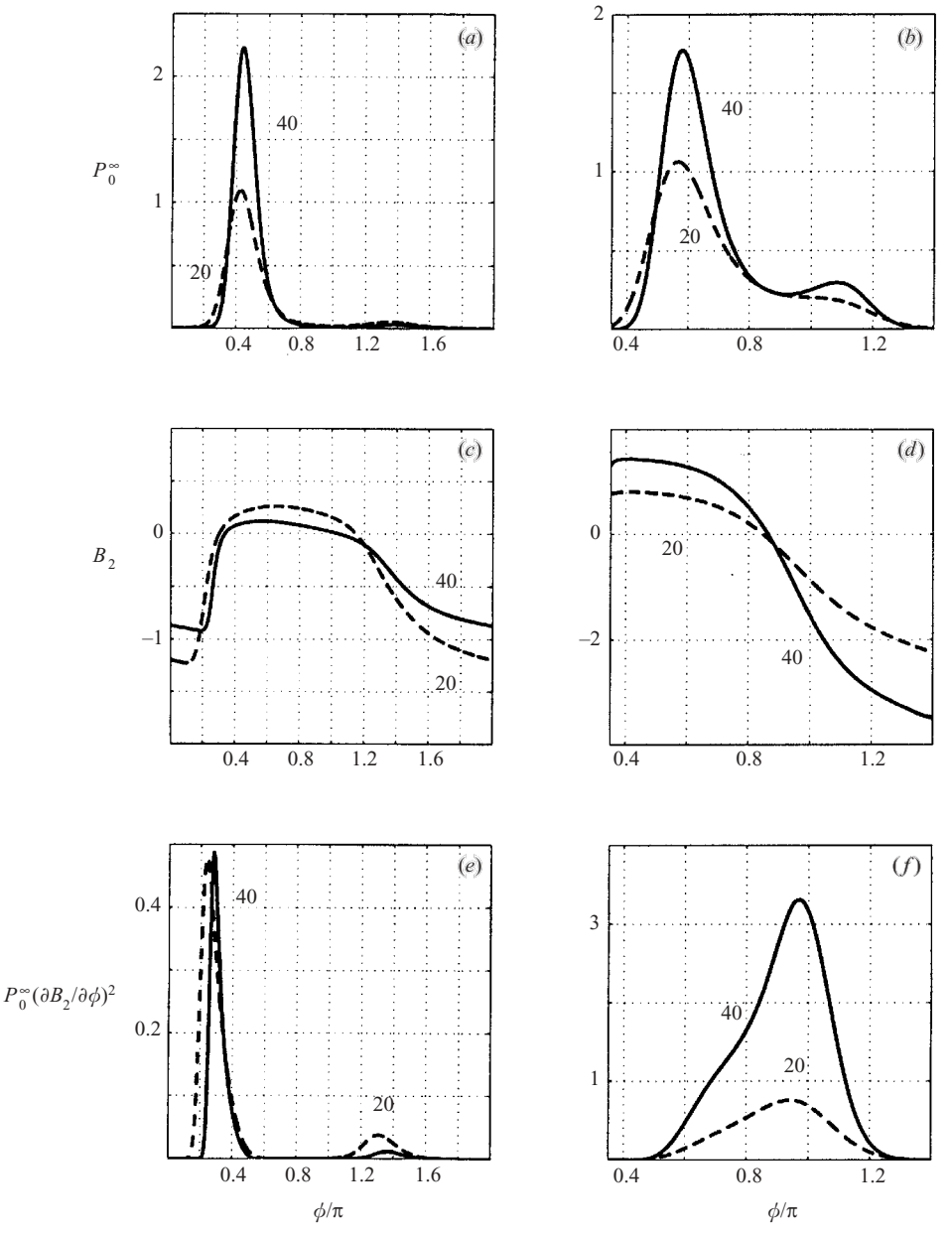

FIGURE 10. Equatorial sections (at $\theta = \pi/2$) of (a, b) P_0^∞, (b, c) B_2 and (d, e) $P_0^\infty(\partial B_2/\partial\phi)^2$ for axisymmetric cells ($B = 0.8$), ———, $Pe = 40$; - - -, $Pe = 20$; (a, c, e) $\phi_f = 60^\circ$ and $\lambda = 0.3$, (b, d, f) $\phi_f = 95^\circ$ and $\lambda = 0.8$.

are purely imaginary (which, in turn, assures that passive advection in the ambient shear field is a slow process relative to orientational relaxation, cf. Frankel & Brenner 1991). We have therefore focused on the simple shear flow (2.17).

In actual bioconvection problems, suspension velocity fields are neither steady nor homogeneous. The present scheme therefore constitutes a local quasi-homogeneous and quasi-steady macroscopic description provided that the ambient velocity gradient is slowly varying on macroscopic length (L) and time (T) scales which are both large

relative to the corresponding scales characterizing the (microscopic) relaxation in orientation space. (Similar scale-disparity arguments are also inherent in asymptotic schemes leading to diffusion approximations in transport problems based on different microscopic models, cf. Hillen & Othmer 2000). Experimental observations of bioconvection (Kessler 1986; Bees & Hill 1997) indicate that $L \approx (1-5)\,\mathrm{mm}$ and $T \approx 1\,\mathrm{min}$. As mentioned following (2.7), orientational relaxation takes place on the time scale $\approx d_r^{-1}$. During this time, the gyrotactic cells swim a horizontal distance $\approx U d_r^{-1} |\bar{\boldsymbol{e}} \times \hat{\boldsymbol{F}}|$ across the essentially vertical streamlines. We have previously estimated $Pe \approx 15$, $\lambda \approx 0.15$ at fully developed bioconvection. Hence, for spherical cells we obtain $|\bar{\boldsymbol{e}} \times \hat{\boldsymbol{F}}| \approx 0.2$ (see figure 2). For a typical swimming speed $U \approx 100\,\mu\mathrm{m\,s^{-1}}$ (Pedley *et al.* 1988) and adopting the value $d_r \approx 0.067\,\mathrm{s^{-1}}$ mentioned earlier, we see that both of the above scale-disparity requirements are reasonably satisfied in bioconvection of gyrotactic cells (cf. Pedley & Kessler 1990).

The present contribution has been motivated by the evidence indicating the sensitivity of the results of simulations of fully developed bioconvection (e.g. Ghorai & Hill 2000) as well as linear stability analyses (cf. Bees & Hill 1998) to the value of the dispersivity $\bar{\boldsymbol{D}}$ and by the lack of rigorous calculations of this effective transport coefficient in suspensions of non-spherical cells at substantial shear rates (Pedley & Kessler 1990, 1992). Accordingly, we have applied the generalized Taylor dispersion theory to the calculation of $\bar{\boldsymbol{U}}$ and $\bar{\boldsymbol{D}}$ which has enabled a systematic study of the respective effects of external field and shear rates on the transport processes in sheared suspensions of swimming gyrotactic micro-organisms. Some of the results (e.g. the non-monotonical variation of dispersion rate with external-field intensity at strong shear, cf. figures 4 and 7) are counter-intuitive. Particularly remarkable are the large dispersion rates predicted in the intermediate regime of external field directions and intensities in suspensions of axisymmetric cells (see figure 9). This seemingly esoteric result may be relevant to the study of gyrotactic plumes where macroscopic convection velocities are nearly vertical.

It is worth considering the relation between the present (2.11) or (2.12) and previous calculations of $\bar{\boldsymbol{D}}$. The starting point of Pedley & Kessler (1990) is the expression of $\bar{\boldsymbol{D}}$ as the limit when $t \to \infty$ of the time integral of the swimming-velocity covariance

$$\bar{\boldsymbol{D}} = \lim_{t\to\infty} \int_0^t \langle [\![\Delta \boldsymbol{U}(t) \Delta \boldsymbol{U}(t_1)]\!]^s \rangle \, \mathrm{d}t_1, \tag{5.1}$$

in which $\langle \cdot \rangle$ denotes an appropriate Lagrangian tracer average. This expression is based on a linear (in t) asymptotic long-time behaviour of the variance $\langle \boldsymbol{R}\boldsymbol{R} \rangle - \langle \boldsymbol{R} \rangle \langle \boldsymbol{R} \rangle$ of the tracer physical-space position (cf. Dill & Brenner 1983; Koch & Brady 1987) and is therefore only valid in the absence of shear. For all (however small) $\boldsymbol{G} \neq 0$, a consistent calculation of the rate of change of $\boldsymbol{R} - \langle \boldsymbol{R} \rangle$ involves the effect of advection in the ambient shear associated with the instantaneous tracer displacement relative to the average position. This, in turn, results in a nonlinear long-time variation of the variance with t (Frankel & Brenner 1991).

To simplify the calculation Pedley & Kessler (1990) postulated a constant direction correlation time to replace (5.1) by the long-time limit of the swimming velocity variance which in present notation is

$$\bar{\boldsymbol{D}} = \tau \int_{S_2} P_0^\infty(\boldsymbol{e}) \Delta \boldsymbol{U}(\boldsymbol{e}) \Delta \boldsymbol{U}(\boldsymbol{e}) \, \mathrm{d}^2\boldsymbol{e} \tag{5.2a}$$

$$= U^2 \tau \int_{S_2} P_0^\infty(\boldsymbol{e}) (\boldsymbol{e}\boldsymbol{e} - \bar{\boldsymbol{e}}\bar{\boldsymbol{e}}) \, \mathrm{d}^2\boldsymbol{e}. \tag{5.2b}$$

In the absence of shear, Dill & Brenner (1983) demonstrated the equivalence of (5.1) and

$$\int_{S_2} P_0^{\infty}(\boldsymbol{e})[\![\Delta \boldsymbol{U}(\boldsymbol{e})\boldsymbol{B}(\boldsymbol{e})]\!]^s \, \mathrm{d}^2\boldsymbol{e}. \tag{5.3}$$

Comparison of (5.2*a*) and (5.3) reveals that the former approximation essentially consists of the (*ad hoc*) replacement of $P_0^{\infty}\boldsymbol{B}$ by $P_0^{\infty}\Delta\boldsymbol{U}$, the corresponding forcing term of the $\boldsymbol{B}(\boldsymbol{e})$-equation (2.15), multiplied by the direction correlation time τ. From a kinematic point of view, (5.2*a*) attempts to express $\bar{\boldsymbol{D}}$ exclusively in terms of instantaneous swimming velocities, whereas (cf. Frankel & Brenner 1991) the rate of dispersion depends on the instantaneous physical-space configuration of the suspension (effectively represented by $\boldsymbol{B}(\boldsymbol{e})$ – see the footnote pertaining to (2.15)–(2.16)) as well. In view of this, the difficulties encountered in estimating or selecting the appropriate value of τ in a consistent interpretation of empirical data (Pedley & Kessler 1990; Bees & Hill 1997, 1998) are expected.

Finally, the calculation by Hill & Bees (2002) of the dispersion of spheres makes use of (5.3). At strong shear, this expression may not be positive definite which is a necessary attribute for $\bar{\boldsymbol{D}}$ to qualify as an effective phenomenological coefficient appearing in the constitutive equation ((2.9) or (1.2)) in a well-posed model problem (Frankel & Brenner 1991, 1993). Furthermore, the difference between the present $\bar{\boldsymbol{D}}$ ((2.11) or (2.12)) and (5.3), i.e. the second term on the right-hand side of (2.11), constitutes in certain cases the dominant contribution to ν at large Pe (see Appendix).

To illustrate the difference between the present calculation and that of Hill & Bees (2002), figure 11 compares the variation of $\bar{\boldsymbol{D}}$ with Pe for spherical cells ($B=0$) in the absence of an external field ($\lambda=0$) (for which case exact closed-form results are obtained in the Appendix) as obtained from (2.11) (solid curves) and (5.3) (dotted lines), respectively. Figure 11(*a*) presents the eigenvalues $\nu_1 > \nu_2$ corresponding to eigenvectors in the plane of shear. We first note that the smaller eigenvalue ν_2, resulting from (5.3), turns negative at $Pe \gtrsim 10$, whereas the present ν_2 remains non-negative for all Pe. Another conspicuous feature is that at intermediate values of Pe, the present ν_1 is nearly twice as large as its counterpart calculated from (5.3). The respective principal azimuthal directions ϕ_1 corresponding to ν_1 according to both (2.11) and (5.3) are presented in figure 11(*b*). They grow markedly different from each other with increasing Pe. At large Pe, these directions become $\pi/4$ apart.

The experimental observations of Hill & Häder (1997) and Vladimirov *et al.* (2000) indicate considerable scatter in swimming speed of cells. Considering the swimming speed and direction as independent random variables (which assumption is supported by the data of Hill & Häder 1997), U in (2.10) may be viewed as an appropriate average of the swimming speed (Pedley & Kessler 1990). Bees *et al.* (1998) and Bees & Hill (1998) modified the *ad hoc* $\bar{\boldsymbol{D}}$ by introducing the factor $\langle U^2\rangle/\langle U\rangle^2$ in the first term of the integrand of (5.2*b*). It is less straightforward to incorporate this randomness into a consistent calculation of $\bar{\boldsymbol{D}}$. The starting-point of such a desirable extension of generalized Taylor dispersion theory is the replacement of (2.1)–(2.3) by an appropriate Fokker–Planck equation governing evolution of the conditional probability density function in six-dimensional phase-space including the swimming speed as an independent random variable. The requisite extension of the long-time model problem (2.8)–(2.9) may be obtained by assuming a sufficiently rapid relaxation of the distribution of swimming speeds (cf. Chandrasekhar 1943; Brenner & Edwards 1993).

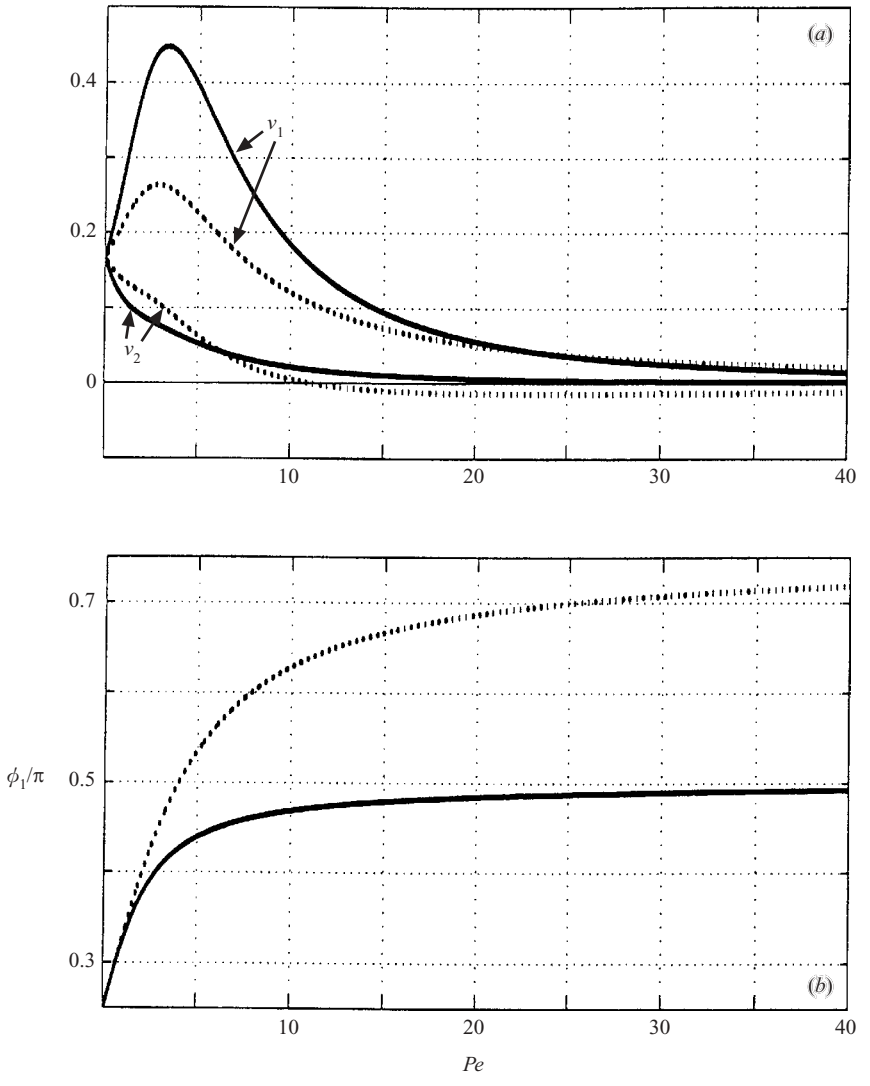

FIGURE 11. Comparison of the variation with *Pe* of (*a*) v and (*b*) $\hat{\boldsymbol{u}}$ for spherical cells in the absence of an external field ($\lambda = 0$) according to ———, (2.11); · · ·, (5.3).

In conclusion, it seems worth noting that the present analysis of the transport of gyrotactic cells subject to gravitational orienting torque may be extended to other types of swimming micro-organisms. Indeed, the present results are applicable whenever the stochastic elements of the rotary motion may effectively be modelled as Brownian rotations and the orienting torque results from the action of a uniform external field on a permanent embedded dipole (e.g. a permanent magnetic dipole, cf. Brenner & Condiff 1974; Rosensweig 1985). In these cases, it is only the physical significance of λ in (2.4) which needs to be reinterpreted. Furthermore, the present generalized Taylor dispersion scheme may readily be adapted (involving relatively minor modifications of (2.10), (2.11), (2.13) and (2.15)) provided that the external 'taxis' may be modelled by an orientation-specific torque.

This work was supported by the fund for the promotion of research at the Technion.

Appendix. Calculation of $\boldsymbol{b}(\boldsymbol{e})$ for spheres

A.1. *Weak external field* ($\lambda \ll 1$)

In the absence of an external field, $\lambda = 0$, spherical particles rotate at the undisturbed fluid angular velocity ($\dot{\theta} = 0$ and $\dot{\phi} = 1/2$ from (2.22a) and (2.22b)), their orientations are uniformly distributed, $P_0^\infty = 1/4\pi$, and hence $\bar{\boldsymbol{e}} = 0$. From (2.20), we thus obtain

$$\tfrac{1}{2}Pe\frac{\partial b_i}{\partial \phi} - \frac{1}{\sin\theta}\frac{\partial}{\partial\theta}\left(\frac{\partial b_i}{\partial\theta}\sin\theta\right) - \frac{1}{\sin^2\theta}\frac{\partial^2 b_i}{\partial\phi^2} - Pe\, b_1\delta_{2i} = \frac{e_i}{4\pi} \quad (i = 1, 2, 3), \tag{A 1}$$

which are to be integrated in conjunction with the normalization conditions (2.20). Excluding singular solutions, b_1 and b_2 are recursively calculated to yield

$$b_1 = \frac{1}{\pi(Pe^2 + 16)}\left(2\cos\phi + \tfrac{1}{2}Pe\sin\phi\right)\sin\theta \tag{A 2}$$

and

$$b_2 = \frac{1}{\pi(Pe^2 + 16)^2}\left[-\tfrac{1}{2}Pe(3Pe^2 - 16)\cos\phi + 2(5Pe^2 + 16)\sin\phi\right]\sin\theta. \tag{A 3}$$

Finally, for b_3, we readily obtain

$$b_3 = \frac{1}{8\pi}\cos\theta. \tag{A 4}$$

From these, the eigenvalue ν and the corresponding principal direction $\hat{\boldsymbol{u}}$, (3.2) and (3.3), are obtained. Following the asymptotic calculation of P_0^∞ in the present limit ($\lambda \ll 1$, $Pe \sim O(1)$) by Brenner & Weissman (1972), we have obtained an $O(\lambda)$ correction to $\boldsymbol{b}$. This correction, however, does not contribute to $\bar{\boldsymbol{D}}$, hence the error estimates in (3.2) and (3.3).

In the discussion following (3.2) and (3.3), the variation of $\hat{\boldsymbol{u}}$ with Pe is mentioned as an indication of a change in the mechanism of dispersion. Owing to the symmetry of $\bar{\boldsymbol{D}}$ about the plane of shear, the principal direction $\hat{\boldsymbol{u}}$ (3.3) is determined by $x = (D_{22} - D_{11})/D_{12}$. To clarify the variation with Pe of this parameter it is useful to represent b_2 by the sum

$$b_2 = b_2^{(1)} + b_2^{(2)}, \tag{A 5}$$

in which (cf. (2.20a))

$$\mathscr{L}b_2^{(1)} = P_0^\infty(e_2 - \bar{e}_2), \tag{A 6}$$

$$\mathscr{L}b_2^{(2)} = Pe\, b_1 \tag{A 7}$$

and both $b_2^{(1)}$ and $b_2^{(2)}$ satisfy the normalization condition (2.20b). When calculating D_{ij} exclusively on the basis of $b_2^{(1)}$, we obtain $x \equiv 0$ which, in turn, yields $\hat{\boldsymbol{u}}^{(1)}$ coinciding with the principal direction of ambient extension at all Pe. When the contribution of $b_2^{(2)}$ is incorporated into the calculation of $\bar{\boldsymbol{D}}$, we obtain $x = Pe$ which results in the rotation of $\hat{\boldsymbol{u}}$ towards the direction of the ambient-fluid velocity. The latter rotation of $\hat{\boldsymbol{u}}$ is thus a manifestation of the emerging prominence (with increasing Pe) of the contribution to dispersion of the coupling (through $\boldsymbol{b}\cdot\boldsymbol{G}$) of b_1 and b_2.

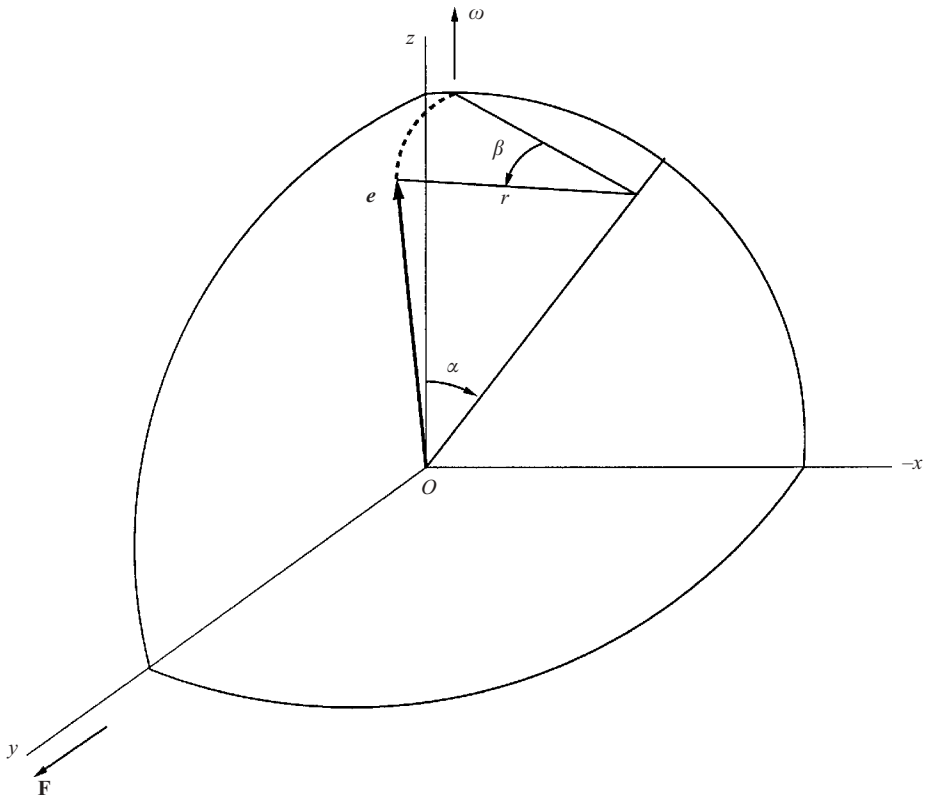

FIGURE 12. Definition of the 'natural' (α, β) coordinate system.

A.2. *Weak Brownian rotations* ($Pe \gg 1, \lambda < 1/2$)

As mentioned at the beginning of § 3, when $\lambda < 1/2$, the rotary motion of dipolar spheres is periodic along a family of circular orbits on S_2. Similarly to Hinch & Leal (1972) we make use of this family as a basis for the system of 'natural' coordinates α (the orbit parameter), the polar angle of the axis about which the particle dipole rotates and β, the phase angle measured along the specific orbit ($\beta = 0$ corresponding to the orbit point closest to the polar axis in the direction of undisturbed fluid vorticity, see figure 12). Parameterizing $\boldsymbol{e}$ in terms of (α, β), Hinch & Leal (1972) obtained

$$P_0^{\infty} \sim \frac{2\lambda A(\lambda)}{\left[\cos\alpha + (4\lambda^2 - \sin^2\alpha)^{1/2}\cos\beta\right]^2 [2 + 4\lambda^2 - 3\sin^2\alpha]} + O(Pe^{-1}), \tag{A 8}$$

with the normalization factor $A(\lambda)$

$$A(\lambda) = (1 - 4\lambda^2)(2 + 4\lambda^2)^{1/2} \left[2\pi \ln \frac{(2 + 4\lambda^2)^{1/2} + 2\lambda}{(2 + 4\lambda^2)^{1/2} - 2\lambda}\right]^{-1}. \tag{A 9}$$

The requisite Cartesian components of $\bar{\boldsymbol{e}}$ are readily obtained

$$\bar{e_1} \sim |\bar{\boldsymbol{e}}| \sin\phi_f + O(Pe^{-1}), \quad \bar{e_2} \sim -|\bar{\boldsymbol{e}}| \cos\phi_f + O(Pe^{-1}), \tag{A 10}$$

wherein

$$|\bar{\boldsymbol{e}}| = \frac{1}{2\lambda}\left[-1 + \frac{4\pi A}{2[3(2+4\lambda^2)]^{1/2}} \ln \frac{(2+4\lambda^2)^{1/2} + 2(3)^{1/2}\lambda}{(2+4\lambda^2)^{1/2} - 2(3)^{1/2}\lambda}\right] \tag{A 11}$$

(Hinch & Leal 1972).

Substituting the expansions

$$b_1 \sim b_1^{(0)} + O(Pe^{-1}), \quad b_2 \sim Pe\, b_2^{(0)} + O(1), \quad b_3 \sim b_3^{(0)} + O(Pe^{-1}), \tag{A 12}$$

into (2.15)–(2.16) we obtain the leading-order equations

$$\nabla_{\boldsymbol{e}} \cdot \left(\dot{\boldsymbol{e}} b_i^{(0)}\right) = 0 \quad (i = 1, 2, 3), \tag{A 13}$$

together with the corresponding normalization conditions

$$\int_{S_2} b_i^{(0)}\, \mathrm{d}^2 e = 0 \quad (i = 1, 2, 3). \tag{A 14}$$

Writing the former in the natural coordinates we obtain

$$\frac{\partial}{\partial \beta}\left\{\frac{\left[\cos\alpha + (4\lambda^2 - \sin^2\alpha)^{1/2}\cos\beta\right]^2}{2\lambda} b_i^{(0)}\right\} = 0 \quad (i = 1, 2, 3), \tag{A 15}$$

which, after integration yield

$$b_i^{(0)} = \frac{2\lambda g_i(\alpha)}{\left[\cos\alpha + (4\lambda^2 - \sin^2\alpha)^{1/2}\cos\beta\right]^2} \quad (i = 1, 2, 3), \tag{A 16}$$

wherein $g_i(\alpha)$ are as yet unknown functions of α.

Following Hinch & Leal (1972), we integrate (2.15) over a domain S of S_2 bounded by the single orbit c. Applying the divergence theorem and making use of the tangency of $\dot{\boldsymbol{e}}$ to c we thus obtain

$$\oint_c \frac{\partial b_1^{(0)}}{\partial n}\, \mathrm{d}l = -\int_S P_0^{\infty}(e_1 - \bar{e}_1)\, \mathrm{d}A, \tag{A 17}$$

$$\oint_c \frac{\partial b_2^{(0)}}{\partial n}\, \mathrm{d}l = -2\int_S b_1^{(0)}\, \mathrm{d}A, \tag{A 18}$$

$$\oint_c \frac{\partial b_3^{(0)}}{\partial n}\, \mathrm{d}l = -\int_S P_0^{\infty} e_3\, \mathrm{d}A, \tag{A 19}$$

in which $\partial/\partial n$ denotes differentiation along an outwardly directed normal to c in a plane tangent to S_2, $\mathrm{d}l$ is an element of arc along c and $\mathrm{d}A$ an areal element on S_2. Expressing (A 17)–(A 19) in terms of (α, β) and substituting (A 16), we obtain the ordinary first-order equations

$$(2 + 4\lambda^2 - 3\sin^2\alpha)\frac{\mathrm{d}g_i}{\mathrm{d}\alpha} - 6\sin\alpha\cos\alpha\, g_i = \frac{(1-4\lambda^2)^{5/2}}{\pi(4\lambda^2 - \sin^2\alpha)} F_i(\alpha) \quad (i = 1, 2, 3), \tag{A 20}$$

wherein the forcing terms are

$$F_1(\alpha) = \frac{\pi A}{(2+4\lambda^2)^{1/2}}\left\{\frac{2}{1-4\lambda^2}\tanh^{-1}\left(\frac{(1-4\lambda^2)^{1/2}}{(2+4\lambda^2)^{1/2}}\tan\alpha\right)\left(\bar{e}_1 + \frac{\sin\phi_f}{2\lambda}\right)\right.$$
$$\left. - \frac{\sin\phi_f}{2(3)^{1/2}\lambda}\ln\frac{(2+4\lambda^2)^{1/2} + 3^{1/2}\sin\alpha}{(2+4\lambda^2)^{1/2} - 3^{1/2}\sin\alpha}\right\}, \tag{A 21a}$$

$$F_2(\alpha) = -\frac{4\pi}{(1-4\lambda^2)^{1/2}} \int_{-\sin^{-1} 2\lambda}^{\alpha} g_1(\alpha_1)\, \mathrm{d}\alpha_1 \tag{A 21b}$$

and

$$F_3(\alpha) = -\frac{\pi A}{2\lambda[3(1-4\lambda^2)]^{1/2}} \ln \frac{\left[3^{1/2}-1\right]\left[3^{1/2}\cos\alpha + (1-4\lambda^2)^{1/2}\right]}{\left[3^{1/2}+1\right]\left[3^{1/2}\cos\alpha - (1-4\lambda^2)^{1/2}\right]}\,. \tag{A 21c}$$

The functions $g_i(\alpha)\,(i=1, 2, 3)$ are thus

$$g_i(\alpha) = \frac{1}{2+4\lambda^2-3\sin^2\alpha} \left\{ \frac{(1-4\lambda^2)^{5/2}}{\pi} \int_{-\sin^{-1} 2\lambda}^{\alpha} \frac{F_i(\alpha_1)}{4\lambda^2-\sin^2\alpha_1}\, \mathrm{d}\alpha_1 + K_i \right\} \quad (i=1, 2, 3). \tag{A 21d}$$

The integration constants obtained from the normalization conditions (A 14) are

$$K_i = -\frac{2\pi A}{(1-4\lambda^2)^{1/2}} \int_{-\sin^{-1} 2\lambda}^{\sin^{-1} 2\lambda} \frac{f(F_i(\alpha))\, \mathrm{d}\alpha}{2+4\lambda^2-3\sin^2\alpha} \quad (i=1, 2, 3) \tag{A 21e}$$

wherein

$$f(F_i(\alpha)) = \frac{(1-4\lambda^2)^{5/2}}{\pi} \int_{-\sin^{-1} 2\lambda}^{\alpha} \frac{F_i(\alpha_1)}{4\lambda^2-\sin^2\alpha_1}\, \mathrm{d}\alpha_1. \tag{A 21f}$$

Substituting the expansions (A 12) into (2.11), we obtain the leading-order approximations of the non-zero scalar components of $\bar{\boldsymbol{D}}$

$$\bar{D}_{11} \sim \int_{S_2} b_1^{(0)} e_1\, \mathrm{d}^2\boldsymbol{e} + O(Pe^{-1}), \quad \bar{D}_{12} \sim \tfrac{1}{2} Pe \int_{S_2} \left[b_2^{(0)} e_1 + \frac{b_1^{(0)^2}}{P_0^{\infty}} \right] \mathrm{d}^2\boldsymbol{e} + O(1),$$

$$\bar{D}_{22} \sim Pe^2 \int_{S_2} \frac{b_1^{(0)} b_2^{(0)}}{P_0^{\infty}}\, \mathrm{d}^2\boldsymbol{e} + O(Pe), \quad \bar{D}_{33} \sim \int_{S_2} b_3^{(0)} e_3\, \mathrm{d}^2\boldsymbol{e} + O(Pe^{-1}).$$

Making use of the above expressions of $b_i^{(0)}$ (A 16) and g_i (A 21*d*) we effect the requisite quadratures in the 'natural' coordinates to obtain for the leading-order approximation

$$\nu_{\infty}(\lambda) = \frac{2\pi \sin^2\phi_f}{A(\lambda)(1-4\lambda^2)^{1/2}} \int_{-\sin^{-1} 2\lambda}^{\sin^{-1} 2\lambda} [f(F_1)f(F_2) + K_2 f(F_1) + K_1 f(F_2) + K_1 K_2] \frac{\mathrm{d}\alpha}{2+4\lambda^2-3\sin^2\alpha} + O(Pe^{-1}) \tag{A 22}$$

in (3.4*a*) and $\hat{\boldsymbol{u}}$ (3.4*b*).

REFERENCES

Almog, Y. & Frankel, I. 1995 The motion of axisymmetric dipolar particles in homogeneous shear flow. *J. Fluid Mech.* **289**, 243–261.

Almog, Y. & Frankel, I. 1998 Rheology of dilute suspensions of Brownian dipolar axisymmetric particles. *J. Fluid Mech.* **366**, 289–310.

Alt, W. 1980 Biased random walk models for chemotaxis and related diffusion approximations. *J. Math. Biol.* **9**, 147–177.

Bearon, R. N. & Pedley, T. J. 2000 Modelling run-and-tumble chemotaxis in a shear flow. *Bull. Math. Biol.* **62**, 775–791.

Bees, M. A. & Hill, N. A. 1997 Wavelengths of bioconvection patterns. *J. Expl Biol.* **200**, 1515–1526.

Bees, M. A. & Hill, N. A. 1998 Linear bioconvection in a suspension of randomly swimming, gyrotactic micro-organisms. *Phys. Fluids* **10**, 1864–1881.

Bees, M. A., Hill, N. A. & Pedley, T. J. 1998 Analytical approximations for the orientation distribution of small dipolar particles in steady shear flows. *J. Math. Biol.* **36**, 269–298.

Brenner, H. 1964 The Stokes resistance of an arbitrary particle – III Shear fields. *Chem. Engng Sci.* **19**, 631–651.

Brenner, H. 1970 Rheology of a dilute suspension of dipolar spherical particles in an external field. *J. Colloid Interface Sci.* **32**, 141–158.

Brenner, H. 1972 Dynamics of neutrally buoyant particles in low Reynolds number flows. *Prog. Heat Mass Transfer* **6**, 509–574.

Brenner, H. 1980 A general theory of Taylor dispersion phenomena. *PhysicoChem. Hydrodyn.* **1**, 91–123.

Brenner, H. 1982 A general theory of Taylor dispersion phenomena II. An extension. *PhysicoChem. Hydrodyn.* **3**, 139–157.

Brenner, H. & Condiff, D. E. 1972 Transport mechanics in systems of orientable particles III. Arbitrary particles. *J. Colloid Interface Sci.* **41**, 228–274.

Brenner, H. & Condiff, D. E. 1974 Transport mechanics in systems of orientable particles IV. Convective transport. *J. Colloid Interface Sci.* **47**, 199–264.

Brenner, H. & Edwards, D. A. 1993 *Macro-transport Processes*, chap. 12. Butterworth–Heinemann.

Brenner, H. & Weissman, M. H. 1972 Rheology of a dilute suspension of dipolar particles in an external field. II. Effects of rotary Brownian motion. *J. Colloid Interface Sci.* **41**, 499–531.

Chandrasekhar, S. 1943 Stochastic problems in physics and astronomy. *Rev. Mod. Phys.* **15**, 1–89.

Dickinson, R. B. 2000 A general transport model for biased cell migration in an anisotropic environment. *J. Math. Biol.* **40**, 97–135.

Dill, L. H. & Brenner, H. 1983 A general theory of Taylor dispersion phenomena VI. Langevin methods. *J. Colloid Interface Sci.* **93**, 343–365.

Frankel, I. & Brenner, H. 1989 On the foundations of generalized Taylor dispersion theory. *J. Fluid Mech.* **204**, 97–119.

Frankel, I. & Brenner, H. 1991 Generalized Taylor dispersion phenomena in unbounded homogeneous shear flows. *J. Fluid Mech.* **230**, 147–181.

Frankel, I. & Brenner, H. 1993 Taylor dispersion of orientable Brownian particles in unbounded homogeneous shear flows. *J. Fluid Mech.* **355**, 129–156.

Ghorai, S. & Hill, N. A. 2000 Periodic arrays of gyrotactic plumes in bioconvection. *Phys. Fluids* **12**, 5–22.

Hall, W. F. & Busenberg, S. N. 1969 Viscosity of magnetic suspensions. *J. Chem. Phys.* **51**, 137–144.

Hill, N. A. & Bees, M. A. 2002 Taylor dispersion of gyrotactic swimming micro-organisms in a linear flow. *Phys. Fluids* **14**, 2598–2605.

Hill, N. A. & Häder, D.-P. 1997 A biased random walk model for the trajectories of swimming micro-organisms. *J. Theor. Biol.* **186**, 503–526.

Hillen, T. & Othmer, H. G. 2000 The diffusion limit of transport equations derived from velocity-jump processes. *SIAM J. Appl. Maths* **61**, 751–775.

Hinch, E. J. & Leal, L. G. 1972 Note on the rheology of a dilute suspension of dipolar spheres with weak Brownian couples. *J. Fluid Mech.* **56**, 803–813.

Jones, M. S., Le Baron, L. & Pedley, T. J. 1994 Biflagellate gyrotaxis in a shear flow. *J. Fluid Mech.* **281**, 137–158.

Kessler, J. O. 1985 Co-operative and concentrative phenomena of swimming micro-organisms. *Contemp. Phys.* **26**, 147–166.

Kessler, J. O. 1986 The external dynamics of swimming micro-organisms. In *Progress in Phycological Research*, vol. 4 (ed. F. E. Round & D. J. Chapman), pp. 257–307. Biopress.

Koch, D. L. & Brady, J. F. 1987 The symmetry properties of the effective diffusivity in anisotropic porous media. *Phys. Fluids* **30**, 642–650.

Manela, A. 2002 Dispersion in shear flows of dilute suspensions of dipolar particles. MSc thesis, Technion–IIT, Israel.

Othmer, H. G., Dunbar, S. R. & Alt, W. 1988 Models of dispersal in biological systems. *J. Math. Biol.* **26**, 263–298.

Pedley, T. J., Hill, N. A. & Kessler, J. O. 1988 The growth of bioconvection patterns in a uniform suspension of gyrotactic micro-organisms. *J. Fluid Mech.* **195**, 223–237.

Pedley, T. J. & Kessler, J. O. 1987 The orientation of spheroidal micro-organisms swimming in a flow field. *Proc. R. Soc. Lond.* B **231**, 47–70.

Pedley, T. J. & Kessler, J. O. 1990 A new continuum model for suspensions of gyrotactic micro-organisms. *J. Fluid Mech.* **212**, 155–182.

Pedley, T. J. & Kessler, J. O. 1992 Hydrodynamic phenomena in suspensions of swimming micro-organisms. *Annu. Rev. Fluid Mech.* **24**, 313–358.

Rosensweig, R. E. 1985 *Ferrohydrodynamics.* Cambridge University Press.

Strand, S. R. & Kim, S. 1992 Dynamics and rheology of a dilute suspension of dipolar nonspherical particles in an external field: Part 1, Steady shear flows. *Rheol. Acta* **31**, 94–117.

Vladimirov, V. A., Denissenko, P. V., Pedley, T. J., Wu, M. & Moskalev, I. S. 2000 Algal motility measured by a laser-based tracking method. *Mar. Freshwater Res.* **51**, 589–600.